ตัวเร่งปฏิกิริยาสององค์ประกอบของนิเกิลออกไซด์และแมงกานีสออกไซด์สำหรับไบโอเซนเซอร์แบบแอมเปอโรเมตริก

นางสาวซุไรนิ บินติ อิบราฮิม

วิทยานิพนธ์นี้เป็นส่วนหนึ่งของการศึกษาตามหลักสูตรปริญญาวิศวกรรมศาสตรดุษฎีบัณฑิต
สาขาวิชาวิศวกรรมไฟฟ้า ภาควิชาวิศวกรรมไฟฟ้า
คณะวิศวกรรมศาสตร์ จุฬาลงกรณ์มหาวิทยาลัย
ปีการศึกษา 2558

BINARY NiO-MnO CATALYST FOR AMPEROMETRIC BIOSENSORS

Miss Suriani Binti Ibrahim

A Dissertation Submitted in Partial Fulfillment of the Requirements
for the Degree of Doctor of Philosophy Program in Electrical Engineering
Department of Electrical Engineering
Faculty of Engineering
Chulalongkorn University
Academic Year 2015

Thesis Title	BINARY NiO-MnO CATALYST FOR AMPEROMETRIC BIOSENSORS
By	Miss Suriani Binti Ibrahim
Field of Study	Electrical Engineering
Thesis Advisor	Associate Professor Mana Sriyudthsak, Ph.D.
Thesis Co-Advisor	Professor Eiry Kobatake, Ph.D.

Accepted by the Faculty of Engineering, Chulalongkorn University in Partial Fulfillment of the Requirements for the Doctoral Degree

.....Dean of the Faculty of Engineering
(Professor Dr Bundhit Eua-arporn)

THESIS COMMITTEE

.....Chairman
(Assistant Professor Arporn Teeramongkonrasmee, Ph.D.)
.....Thesis Advisor
(Associate Professor Mana Sriyudthsak, Ph.D.)
.....Thesis Co-Advisor
(Professor Eiry Kobatake, Ph.D.)
.....Examiner
(Associate Professor Tawatchai Charinpanitkul, Ph.D.)
.....Examiner
(Assistant Professor Chanchana Tangwongsan, Ph.D.)
.....External Examiner
(Sitthisuntorn Supothina, Ph.D.)

ซุไรนิ บินติ อิบราฮิม : ตัวเร่งปฏิกิริยาสององค์ประกอบของนิเกิลออกไซด์และแมงกานีสออกไซด์สำหรับไบโอเซนเซอร์แบบแอมเปอโรเมตริก (BINARY NiO-MnO CATALYST FOR AMPEROMETRIC BIOSENSORS) อ.ที่ปรึกษาวิทยานิพนธ์หลัก: รศ. ดร.มานะ ศรียุทธศักดิ์, อ.ที่ปรึกษาวิทยานิพนธ์ร่วม: ศ. ดร.เอรี คูบาตาเกะ, 105 หน้า.

มีการนำออกไซด์ของโลหะในกลุ่มทรานสิชันไปใช้งานในกระบวนการเร่งปฏิกิริยาที่สำคัญอย่างกว้างขวาง ในวิทยานิพนธ์นี้ได้สังเคราะห์ออกไซด์ของโลหะในกลุ่มทรานสิชันจำนวนสองชนิดคือนิเกิลออกไซด์และแมงกานีสออกไซด์โดยวิธีไฮโดรเทอร์มอล ได้ศึกษาลักษณะสมบัติของสารทั้งสองชนิดด้วยเครื่อง BET กล้องจุลทรรศน์อิเล็กตรอนแบบส่องผ่าน การเลี้ยวเบนของรังสีเอ็กซ์ ฟูเรียร์ทรานสฟอร์มอินฟราเรดสเปคโตรสโคปี และรามานสเปคโตรสโคปี จากการศึกษาพบว่ารูปแบบของนิเกิลออกไซด์และแมงกานีสออกไซด์มีลักษณะเป็นเส้นใยและทรงกลมระดับนาโนเมตรตามลำดับ ขนาดของพื้นที่ผิวของอนุภาคจะขึ้นกับความเข้มข้นของสารตั้งต้น อุณหภูมิและระยะเวลาการให้ความร้อน พบว่านิเกิลออกไซด์และแมงกานีสออกไซด์ที่ได้จะมีพื้นที่ผิวสูงสุดเป็น 92.3 และ102.9 ตารางเมตรต่อกรัมเมื่อใช้นิเกิลอะซีเตตความเข้มข้น 0.3 M และแมงกานีสอะซีเตตความเข้มข้น 0.5 M เป็นสารตั้งต้น โดยให้ความร้อนที่อุณหภูมิ 200 และ 100 องศาเซลเซียส เป็นเวลา 7 และ 3 ชั่วโมงตามลำดับ จากนั้นได้นำออกไซด์ของโลหะที่มีขนาดระดับนาโนเมตรทั้งสองไปสร้างไบโอเซนเซอร์สำหรับวัดไฮโดรเจนเปอร์ออกไซด์ การเตรียมทำโดยนำอนุภาคของออกไซด์ของโลหะ โพลีโดปามีน และท่อคาร์บอนนาโนมาเคลือบทีละชั้นบนขั้วไฟฟ้าทอง พบว่าเมื่อใช้ท่อคาร์บอนนาโน นิเกิลออกไซด์และแมงกานีสออกไซด์ในการปรับแต่งผิวของขั้วไฟฟ้าทองจะเพิ่มการตอบสนองในการวัดแบบโวลแทมเมตรีได้อย่างมาก ขั้วไฟฟ้าทองที่ปรับแต่งด้วยนิเกิลออกไซด์ แมงกานีสออกไซด์ และเอนไซม์เปอร์ออกซิเดสจะให้การตอบสนองในการวัดแบบแอมเปอโรเมตรีได้สูงสุด ซึ่งคาดว่าเป็นผลของการเร่งปฏิกิริยาการสลายไฮโดรเจนเปอร์ออกไซด์ของตัวเร่งปฏิกิริยาทั้งสองร่วมกับเอนไซม์ โดยสามารถวัดไฮโดรเจนเปอร์ออกไซด์ได้ในช่วงความเข้มข้น 32 ไมโครโมลาร์ ถึง 3.0 มิลลิโมลาร์

ภาควิชา วิศวกรรมไฟฟ้า	ลายมือชื่อนิสิต .....
สาขาวิชา วิศวกรรมไฟฟ้า	ลายมือชื่อ อ.ที่ปรึกษาหลัก .....
ปีการศึกษา 2558	ลายมือชื่อ อ.ที่ปรึกษาร่วม .....

5471462721 : MAJOR ELECTRICAL ENGINEERING
KEYWORDS: HYDROTHERMAL REACTION / HYDROGEN PEROXIDE / NICKEL OXIDE / MANGANESE OXIDE / CATALYST

SURIANI BINTI IBRAHIM: BINARY NiO-MnO CATALYST FOR AMPEROMETRIC BIOSENSORS. ADVISOR: ASSOC. PROF. MANA SRIYUDTHSAK, Ph.D., CO-ADVISOR: PROF. EIRY KOBATAKE, Ph.D., 105 pp.

Transition metal oxides are used in a wide variety of technologically important catalytic processes. In this work, two types of transition metal oxides, nickel oxide and manganese oxide, were synthesized using hydrothermal technique. They were subjected to material characterization testing such as Brunaer-Emmett-Teller (BET), transmission electron microscope (TEM), X-ray diffraction (XRD), Fourier transform infrared spectroscopy (FTIR) and Raman spectroscopy. It was found that the morphology of nickel oxide and manganese oxide were nanowires and nano - spherical, respectively. The surface area of the particles were found to be affected by the starting material concentration, heating temperature and heating time. It was found that the highest surface area of nickel oxide and manganese oxide, 92.3 $m^2 g^{-1}$ and 102.9 $m^2 g^{-1}$, were obtained when 0.3 M nickel acetate and 0.5 M manganese acetate were used as starting material and synthesized at 200 °C and 100 °C for 7 hours and 3 hours, respectively. The both materials were then applied to construct amperometric biosensors for hydrogen peroxide detection. Layer by layer modified gold electrodes were fabricated by using the metal oxide nanoparticle, polydopamine and carbon nanotubes. The voltammetric responses greatly improved when carbon nanotubes, nickel oxide and manganese oxide were added on the modified gold electrodes. Modified gold electrodes with metal oxides and horseradish peroxidase showed the highest amperometric response. This is due to catalysis activity of both the binary catalyst and enzyme on hydrogen peroxide decomposition. The dynamic range for hydrogen peroxide detection was obtained from 32 μM – 3.0 mM.

Department:	Electrical Engineering	Student's Signature	.....
Field of Study:	Electrical Engineering	Advisor's Signature	.....
Academic Year:	2015	Co-Advisor's Signature	.....

ACKNOWLEDGEMENTS

Firstly I would like to acknowledge my supervisor, Assoc. Prof. Dr. Mana Sriyudstak for accepted me as his student at Bio-Electronic Research Laboratory. Many thanks for his guidance, assistance and patience during my study at Chulalongkorn University.

My special thank goes to my labmates in Bio-Electronic Research Laboratory for their help, assistance and patience during my study. I would like to acknowledge Department of Electrical Engineering, Faculty of Engineering, Chulalongkorn University for their support and assistance during my study.

I also want to acknowledge my co-advisor Prof. Dr.. Eiry Kobatake at Tokyo Institute Technology for allowed me to do 3 months training at his lab. Special thank goes to Dr Mie and Dr Mashimo for their help and assistance on my experiment works. I also would like to thanks all my labmates for their assistances during my stay at Japan.

I also would like to acknowledge Assoc. Prof. Dr. Tawatchai Charinpanitkul from Department of Chemical Engineering for his advises and assistance during nanomaterials synthesized. Many thanks also for Prof. Dr. Suthichai Assabumrungrat, Assoc. Prof. Dr. Patama Visuttipitukul and Mr. Decho Thong-Aram from Faculty of Engineering for their assistance during nanomaterials characterization.

My special gratitude also goes to AUNSeed-Net sponsorship under Japan International Cooperation Agency (JICA) for providing scholarship, conference support and research fund during my study at Thailand and Japan.

Finally and the most important I would like to acknowledge my parent Ibrahim and Zainum and all my brothers, Nazri, Azman and Shukri for their support and understanding during my study.

CONTENTS

Page

Page

Page

List of Figures

Page

List of Tables

Abbreviation

HRP	Horseradish Peroxidase
H_2O_2	Hydrogen Peroxide
AH_2	aromatic electron donor
AH*	one electron oxidation product
ROS	reactive oxygen species
N	moles
Q	electroactive species reacted and the charge passed through the sensor
n	number of electrons transferred
F	Faraday constant
E	cell potential
E_0	standard cell potential
z	number of moles of electrons transferred in the cell reaction
a_{Red}	chemical activities for the reductant species
a_{Ox}	chemical activities for the oxidant species
NIOSH	National Institute for Occupational Safety and Health
IDLH	Immediately dangerous to life and health limit
ppm	part per million
J	net flow of the matter
dc/dx	concentration gradient
k*	heterogeneous kinetic constant
K_E'	diffusion constant
v	effective frequency along the reaction coordinate
α	electron transfer coefficient
r	distance
G_0	activation energy
d_0	Van der Waals distance
d	real distance donor-acceptor
BET	Brunaer-Emmett-Teller
XRD	X-Ray Diffraction
TEM	Transmission Electron Microscope
QCM	Quartz crystal microbalance
p	equilibrium pressure of adsorbates at the temperature of adsorption
p_0	saturation pressure of adsorbates at the temperature of adsorption
v	adsorbed gas quantity
v_m	monolayer adsorbed gas quantity
c	BET constant
E_1	heat of adsorption for the first layer
E_L	heat of adsorption for the second and higher layers
S_{total}	total surface area
S_{BET}	specific surface area

v_m	volume
N	Avogadro's number
s	adsorption cross section of the adsorbing species
V	molar volume of the adsorbate gas
D_v	volume weighted crystallite size
K	Scherrer constant
λ	wavelength of radiation
β	full-width at half maximum
n	number of electrode
A	electrode area (cm^2)
C	concentration

Chapter 1
Introduction

Nanotechnology is any technology that involved small size of materials (< 100 nm). Nanomaterials display unique physical, chemical and electronic depending on size and shapes. One of the important characterizations of nanomaterials is large surface area. Therefore nanomaterials have been usually used in sensor to increase sensitivity, lower the detection limit and lower volume of samples to analyzed [1]. Within nanomaterials, metal and semiconductor are widely used in electrochemical applications. In 20th century, metal oxide catalysts were used widely in petroleum,chemical and environmental industries. Mixed metal oxides catalysts were used in industries as an oxidation catalyst [2]. Metal oxides play important roles in many fields including material science, geology, mechanical and electrical engineering [3]. Metal oxide nanoparticles have unique properties such as high surface area, fast electron transfer and good biocompatibility [4]. The 3 main factors why metal oxides is suitable for catalysis , (i) coordination environment of the surface atoms, (ii) redox properties of the metals oxide, and (iii) oxidation state of the surface [5]. The redox behavior of oxides are related with their acid-base properties. Most of transition metal ions exhibit multiple stable oxidation states. Metal oxides consist of metallic cations and oxygen anions. For example catalysis is the catalytic converter in a car to reduce the toxicity of emission from the car engine. The catalysts such as platinum and manganese are used to convert harmful nitrogen oxides into harmless nitrogen and oxygen. Bimetallic nanoparticles have better properties compare to monometallic nanoparticles due to unique properties of combination 2 or more oxides.

For example, CoPt core-shell nanoalloys have good magnetic properties and had been used as biomedical magnetic sensors and ultrahigh-density memory devices [6]. The bimetallic nanoalloys coordination depend on composition, synthesis route and reaction conditions. A significant application for bimetallic nanoalloys is catalysts [7]. Bimetallic alloys offer a high surface-to-volume ratio and good catalytic activity compare to monometallic materials. Tao et al. used RhPd nanoparticles for pollution abatement by using NO, O_2, H_2 and NO + CO environments [8]. They produced core-shell structure under enviroments tested by using independent model nanoparticles size 15 nm in diameter. Moreover, the RhPd NPs shows excellent performance in Ethanol Steam Reforming ESR ($C_2H_5OH + 3\ H_2O \rightarrow 6H_2 + 2CO_2$) with CeO_2 [9, 10]. This finding is very important to obtain hydrogen from renewable and bioethanol without release any toxicity [11, 12]. To remove chlorinated ethenes, the best material is palladium which act as a hydrodechlorination catalysts. However, this materials shown low catalytic activity and tend to deactivated. Palladium-gold bimetallic exhibit excellent catalyst activity and good in deactivated resistance [13]. This catalyst is a novel material for development in hydrodechlorination catalysis technology.

Besides industrial catalysts, there also have natural catalysts are called enzymes and are found in every living cell. Enzymes are proteins, which are made from amino acids. The catalytic reaction occurs at a particular place in the enzyme, calls active site. Natural catalyst shows very high activity and selectivity, meaning that they are able to make the desired product at a very high rate. Enzymes are less stable than the inorganic catalysts. Consequence they stop catalyzing the reaction

after certain amount of time, which is called deactivation. The lifetime of the enzymes depends on the conditions under which they work.

Dopamine (3,4-dihydroxphenylethylamine) (DA), a catecholamine neurotransmitter, plays a significant physiological role in mammalians. Polydopamine is a simple, inexpensive, and green material. Recently, polydopamine has become potential coating material that have been used in various type of materials. For example, Lee et al. used polydopamine to immobilize trypsin on the various of materials such as copper and cellulose [14]. Li et al. reported by immobilize glucose oxidase with dopamine could maintain bioactivity [15].

Carbon nanotubes (CNTs) have received great attention due to their good combination of mechanical, thermal, chemical, and optical properties [16, 17] Carbon nanotubes have been applied in many research fields including catalysis [18], sorption [19], chemical sensing [20], electrically conducting polymers [21], field emission [22], energy storage [23], molecular electronics [24], and biomaterials [25].

Hydrogen peroxide is very important substance in most of industrial processes and in many biological systems [26]. The unique property of H_2O_2 is oxidizing properties. H_2O_2 was decompose and produced hydroxyl radical. This radical act as oxidizing agents in the degradation of organic pollutants from water for textile industry [27]. This substances are toxic to the human and also animals [27]. Moreover, oxidizing of H_2O_2 plays a significant role in the manufacture of industrial water electrolyzes, secondary metal-air batteries and fuel cells [28]. Regarding medical applications, H_2O_2 is major reactive oxygen species (ROS) in living organisms and plays a central role in causing several life-threatening human diseases

such as cancer, cardiovascular disorders, Alzheimer and related neurodegenerative diseases. Due to these wide and varied applications, an extensive demand for establishing the protocol for H_2O_2 detection is extremely important.

Nowadays, the electrochemical methods are very attractive technique because of inexpensive, high sensitivity and high selectivity to determine of a particular analyte by choosing the appropriate applied potential. The analytical data was obtained from the electrical signal that results from the interaction of the target analyte and the transducer. Amperometric sensors and potentiometric sensors are the types of electrochemical sensors. For this work, electrochemical methods have been used to characterize the performance of the modified gold electrode.

In our work, we will synthesize metal oxides individually by using hydrothermal technique and carbon nanotubes by using chemical vapor deposition techniques. Layer by layer structure thin film were fabricate on the top of the commercial gold electrode. After that, we will characterize the sensor by electrochemical testing to detect hydrogen peroxide.

1.1 Motivation

Hydrogen peroxide is a toxic substance; so it can cause harmful to human life and environments. According to National Institute for Occupational Safety and Health (NIOSH), immediately dangerous to life and health limit (IDLH) is 75 ppm (2.2 mM). Therefore, we need a very high sensitivity sensor to detect the hydrogen peroxide.

1.2 Objectives

The main goal this research is to fabricate and characterize a sensitive biosensor for the hydrogen peroxide detection. A binary catalyst is considered with the assumption that it will increase the sensitivity of the biosensor. Polydopamine will be modified with carbon nanotube to be more conductive With the help of enzyme, the performance of biosensor will be greatly improved. Other objective of this research includes:

1. To synthesize nanomaterials of binary catalyst MnO-NiO using hydrothermal technique.
2. To synthesize carbon nanotube using chemical vapor deposition technique (CVD).
3. To study performance of nanocomposite thin film (PDA-CNT-MnO-NiO-HRP) using materials and electrical characterizations techniques.

1.3 Scope of work

The scope of this research includes:

1. Synthesize the nanomaterials

   MnO and NiO nanomaterials were chosen for this study because of their unique properties such as low cost, high surface area and biocompatibility. Hydrothermal technique is the attractive method to synthesize the nanomaterials due to it its simplicity and low cost. Carbon nanotubes was used to improved properties of polydopamine.

2. Amperometric hydrogen peroxide biosensor fabrication.

   Amperometry is the attractive techniques because of its unique properties such as simple operation, fast detection, low cost and good sensitivity.

1.4 Contribution

The nanocomposite binary catalyst fabricated from this research can be used in detection of low concentrations of H_2O_2. The sensitivity of fabricated sensors were greatly improved when binary catalyst and enzyme were used for hydrogen peroxide detection.

1.5 Thesis outline

This work will present about nanomaterials synthesized and its used in hydrogen peroxide detection.

Chapter 2 Theoretical Aspects

This section will explain the fundamental theory about transition metal oxide, carbon nanotube and hydrogen peroxide sensor and the mechanisms that related to this thesis.

Chapter 3 Methodology

This section will explain about the materials and techniques to synhesize the nanomaterials. After synthesized the nanomaterials, the characterization testing was carried by using FTIR, BET, TEM, Raman, XRD. The process continue with the sensor fabrication by using commercial gold electrodes. Layer by layer film was deposited by using metal oxides catalyst as a first layer and polydopamine mix with carbon nanotube as a second layer. The modified gold sensors were characterized by using electrochemical testings.

Chapter 4 Results and Discussions

This section will explain about physical, chemical and crystal properties for synthesized nanomaterials. Effect of concentration, heating tenperature and heating time during nanomaterials synthesize also will discuss. Performance of hydrogen peroxide biosensors will investigate by calculating total current produced.

Chapter 5 Conclusion and Future Recommendations

This section will summarize the work that had been done for this thesis and any recommendations that can be consider to improve this thesis.

Chapter 2

Theoretical Aspects and Literature Review

This section will discuss about theoretical studies related to this work such as hydrogen peroxide, transition metals oxides, carbon nanotube and electrochemical sensors. This section also discuss about materials characterizations testing methods that will be used to characterize nanoparticles such as Transmission electron microscopy (TEM), Fourier transforms infrared spectroscopy (FTIR), Raman spectroscopy, Brunauer–Emmett–Teller (BET) and X-ray diffraction.

2.1 Catalysts

Catalysts not only had been use in chemical processes but catalyst is very important in human body for enzymatic reactions. In manufacturing, heterogeneous catalyst are widely applied at high temperature application. For low temperature application, they used homogeneous catalyst. For biocatalyst, the temperature for enzyme reaction is around 40 °C and they very selective compare to industrial catalyst. Transition metal oxides normally in particles and dispersed in support materials such as alumina. This combination widely applied in industry as well as in research areas.

2.1.1 Transition metal oxide

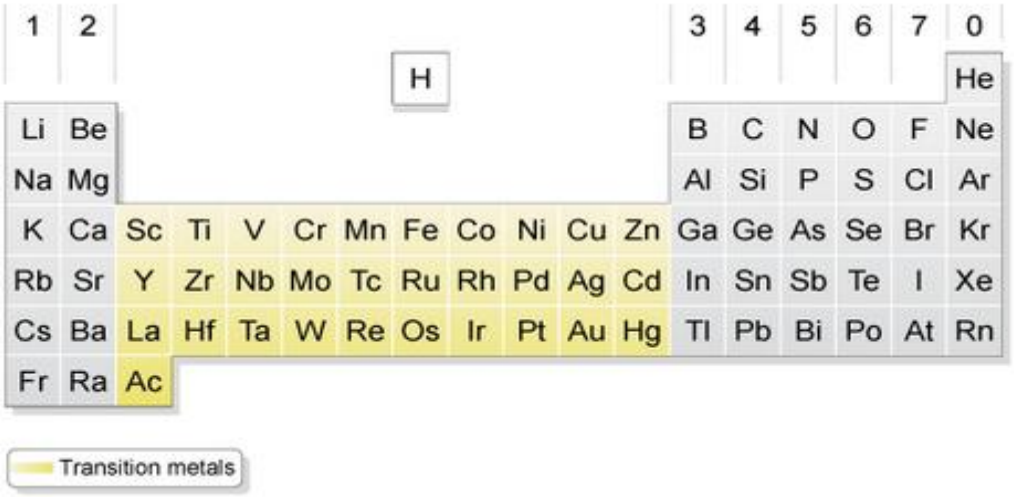

Figure 2.1 Transition metals in periodic table

Figure 2.1 shows all the transition metals position at periodic table [29] . Transition metal oxides are widely used in catalytic processes such as oxidation, reduction and dehydrogenation. These materials have useful electronic and magnetic properties. The IUPAC definition defines a transition metal as "an element whose atom has a partially filled d sub-shell, or which can give rise to cations with an incomplete d sub-shell. The transition metals can be divided in d-block metals, which is 3d elements from Sc to Cu, 4d elements from Y to Ag, and 5d elements from Hf to Au. Some metal like Zn, Cd and Hg not counted as transition metals because they exist in electronic configuration $d^{10}s^2$, with no incomplete d shell [30].

All metals apart from the noble metals are covered by an oxide layer under atmosphere conditions to protect the metallic substrate [31]. At ambient conditions the majority of these oxide layers are terminated by hydroxyl groups and covered with an adsorbed water layer in order to minimize the surface potential [32]. The

thickness, homogeneity and stability of these oxide layers vary for the different metals. The oxide layers are very thin, often only several nanometers thick.

LaVO4, rare earth orthovanadate possess less activity for carbon monoxide oxidation reaction. But when Mn^{4+} was added, the system shown remarkable catalytic activity and structural stability [33]. By introduced Mn4+ in the system, it will generate oxygen and it will be substitute over repetitive redox cycles because of iron substitution [34]. The selective catalytic reduction (SCR) of NO by CO over supported noble metal (Pt, Pd, or Rh) catalysts is expensive. Therefore, it is an important task to find another type of materials to replace noble metals.

Latest study discuss about significant performance of transition metal oxides for reduction of NO by CO [35-39]. Copper oxide has been proven to be the best catalyst material for this reaction [40, 41]. In particular, the $CuO/Ce_{0.8}Zr_{0.2}O_2$ combination catalyst possesses excellent activity for the reduction of NO by CO. The lattice imperfection and some modification on CeO_2 will cause increment redox properties and higher catalytic activity [42]. From all mixed oxides for catalysis application, MnOx-based materials showed the best candidate for oxidation reaction. These oxides were exhibit as a active phases in variety of processes like oxidative coupling of methane [43], CO oxidation [44], ethyl-benzene oxidative dehydrogenation [45, 46], and other classes of catalytic oxidation processes [47-49]. Manganese oxide can exist in variable oxidation state which is influence their catalytic properties (MnO_2, Mn_2O_3, Mn_3O_4, or MnO). Mn is able to play the role of either a reducing agent ($Mn^{2+} - e^- \rightarrow Mn^{3+} - e^- \rightarrow Mn^{4+}$) or an oxidizing agent (Mn^{4+}

+ $e^- \rightarrow Mn^{3+}$ + $e^- \rightarrow Mn^{2+}$).We can identify the present of MnO_x or mixed MnO_2/Mn_2O_3 by study a structural characteristic of unsupported MnO_x. [50-52]. When MnO_x was combined with another materials and this mixture were deposit on the high surface area support showed different catalytic activity [50, 51]. Recent studies reveal that when MnO_2 is added in La_2O_3 or CeO_2, the oxygen mobility from the MnO_x structure is strongly affected to catalytic reaction [53-55]. In Mn – Ce system, Ce will provides oxygen to Mn at low temperature. However at high temperature, it will remove the oxygen. Therefore Ce provides the activity of MnO_x in oxidation processes at lower temperature and decreases its activity at high temperatures [56-59]. Table 2.1 shows metal oxide catalysts used in various applications including hydrogen peroxide detection.

Table 2. 1 Example of metal catalysts used in sensors

Catalyst	Function	Detection range	Authors
NiO_x/TH, NiO_x/CB	H_2O_2 reduction	1µM – 10mM	Abdullah et al. [60]
Ni/Co/NSC	Glucose oxidation	10µM-2.65 mM	Li et al. [61]
PdNi	Glucose and H_2O_2 oxidation	0.05 – 0.95 mM	Zhao et al. [62]
NiO/GR	Reduction of H_2O_2 and trichloroacetic acid	2.13 – 248.2 uMol/L	Sun et al. [63]
NiO/MWCNT/PANI	H_2O_2 oxidation	3 – 700 µM	Suman et al. [64]
MnO_2 nanosheet	H_2O_2 oxidation	$5x10^{-6}$ – 3.5 x 10^{-3} M	Zhang et al. [65]
Pt-MnO_x	H_2O_2 oxidation	2.0 µM – 4.0 mM	Hilal et al. [66]
CuO - graphene	Glucose oxidation	1uM – 8 mM	Yuwei Hou et. al. [67]
MnO_2 - carbon	H_2O_2 oxidation	50 uM – 0.6 mM	Liqiang Luo et al. [68]
Ag – MnO_2 - MWCNTs	H_2O_2 oxidation	5 uM – 10.4 mM	Yang Han et al. [69]
Cu_2O - graphene	Glucose oxidation	0.01 –6 mM	Dan Ling Zhou et al. [70]
Bio - graphene	H_2O_2 oxidation	0.25 – 4.75 mM	Zhiyuan Yu et al. [71]
MnO_2 / Au	H_2O_2 oxidation	5 uM – 10 mM	Yu Jung Yang et al. [72]
FeO_4 @ ZrO_2	H_2O_2 oxidation	0.64 uM – 148 uM	Hua Ping Peng et al. [73]
MnO_2/grapheme/CNT	H_2O_2 oxidation	1 – 1030 uM	Daixin Ye et al. [74]
CuO-sulfur-graphene	Glucose oxidation	0.1 – 10.5 mM	Ye Tian et al. [75]
CuO/ PPy/rGO	Glucose oxidation	0.1 – 100 mM	Pooria Moozarm Nia et al. [76]
Fe_3O_4/MWCNT/PANI	phenolic	0.1 – 10 uM 10 uM – 500 uM	Rachna Rawal et al.[77]
CuO-butyl carbitol acetate	Glucose oxidation	0.78 – 100 mM	Sang Hoo Kim et al. [78]
Au – Fe_3O_4 @ SiO2	Glucose oxidation	0.05 – 1.0 mM 1.0 – 8.0 mM	Xiao Jun Chen et al. [79]
Ni/Cu – TiO_2	Glucose oxidation	1.0 uM – 3.2 mM	Kavitha Thandaran et al. [80]
ZnO - CuO	Glucose oxidation	0.1 – 4167 uM	Chelladurai Karuppiah et al. [81]
CuO	Uric acid	0.05 – 1 mM	Kajal Jindal et al. [82]
NiO - ITO	Urea	0.83 – 16.65 mM	Manisha Tyagi et al. [83]
Graphene-cnt-ZnO	Glucose oxidation	10 uM – 6.5 mM	Kuo Yuan Hwa et al. [84]

2.1.2 Factors that affect the performances of catalyst

There are several factors that affect performance of catalyst, such as:

2.1.2.1 Size of metal nanoparticles

One of the important factors that affect catalyst properties is size. When the surface area of metal increase the catalytic effect also increase. Catalytic reaction will occur on the metal nanoparticle surface, therefore the small size will resulting high surface area and will affect the catalytic activity. There are many studies showed the effect of metal nanoparticles size on the catalytic activity. For example, when size of Rh nanoparticles is decrease the hydrogenation rate of olefins is increase [85]. However, the relationship between catalytic activity and total surface area is not always linear. The rates of hydrogenation for internal and external olefins are different with surface area. This phenomenon might be because of the steric effect or the surface structure effect. Some study reported that the catalytic activity will increase with decreasing particle size until a certain size. The highest activity for Pt nanoparticles are reported at 3 nm for photochemical hydrogen generation [86]. This phenomenon might be because of mechanism of catalysis. Platinum nanoparticles need two-electron reduction for hydrogen generation. Therefore, Pt nanoparticles need to have certain size to maintain numbers of electrons. The selectivity of the catalyst also affect by size of nanoparticles. Study showed that the selectivity of monoene increase with decreasing a Pd nanoparticles size below about 2 nm [87]. This phenomena might be because of steric effect or the surface structure effect of nanoparticle catalysts.

2.1.2.2 Influence of the particular metal complex

The redox processes reaction and is only affected by metal oxides with variable oxidation states. Therefore the redox potential is the important factor that needs to be considered. Normally, when the redox potential is increased, the oxidation rate also increases [88].

2.1.2.3 Temperature

At low temperature, the rate of catalyzed oxidation is quite low compare to high temperature. It is because; at high temperature the chain process can develop rapidly [88].

2.1.2.4 Physicochemical Properties of Metal Catalysts in Solution

Metal catalysts normally combine with carboxylic acid salts (stearates, acetates, naphthenates). Salt will dissociate into ion in a polar solvent. No dissociate will happen if hydrocarbon solvents is used for metal catalyst. When concentration of carboxylic acid salts is increase, it will leads to micelle formation [88].

2.1.2.5 Mixed-metal catalyst-synergism and antagonism

When the 2 catalysts are combined, the rate of reaction is greater than that expected, the action is referred to as synergism. If the result is less than that expected from combination of the separate effects, it is called antagonism. These two effects are often observed in metal-catalyzed auto-oxidations [88].

2.1.3 Horseradish peroxidase (HRP)

Horseradish peroxidase is an enzyme with a molecular weight of about 40,000. Horseradish peroxidase contains two different types of metal centre, iron (III) protoporphyrin IX (usually refer to 'heme group') and 2 calcium atoms [89]. This enzyme catalyzes the oxidation of hydrogen peroxide. The sequence of events involved in this catalysis is quite well understood as the result of the work of Keilin and Nichols [90]. The heme group will be participated in reaction with hydrogen peroxide in electrochemical process for this work. Figure 2.2 show some essential structure of horseradish peroxidase [91].

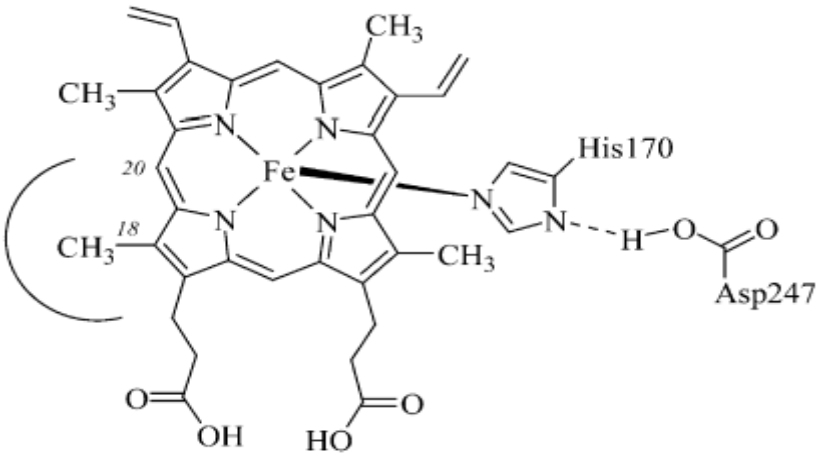

Figure 2. 2 Essential structure of horseradish peroxidase

The formation of catalytic intermediates of HRP with H_2O_2 to form compound I and compound II was studied in great detail by Theorell, George, Chance and Keilin [90, 92, 93]. HRP will reacts with H2O2 and form transient green complex, compound I. After that, compound II were formed resulting from reduction process. Later, compound II will reduce one-electron to generate ferriperoxidase and start a new cycle again. The reactions as follows [91]:

Fe^{3+}-HRP + H_2O_2 →Compound I + H_2O (1)

Compound I + AH_2→Compound II + AH (2)

Compound II + AH_2→Fe^{3+}-HRP + AH (3)

AH*+AH*→ A + AH_2 (4)

where AH_2 is aromatic electron donor and AH* is one electron oxidation product (free radical). The radicals will combine to generate stable oxidation product A. The formation of compound I occurs by heterolytic cleavage of the O-O bond of H_2O_2 through an electron "push pull" mechanism. The positive distal histidine imidazole (His-42) provides the pull and a partially or fully deprotonated proximal histidine (His-170) provides the push. The reduction of compound I to compound II by aromatic electron donor is related with proton transfer from donor to the imidazole nitrogen of distal His-42. Further compound II were reduced to ferric state by another donor molecule. Figure 2.3 show chemical structures for compound I and compound II for horseradish peroxidase [91].

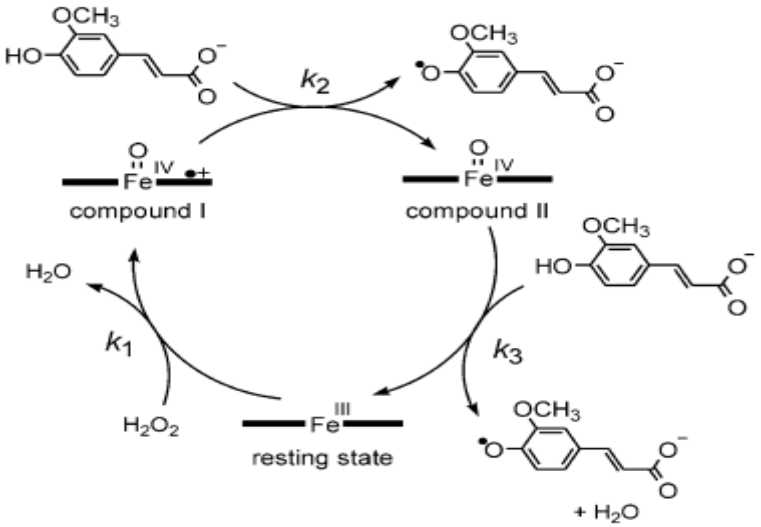

Figure 2. 3 Compound I and Compound II for horseradish peroxidase

The electron transfer properties of enzymes to electrodes surface is an important factor for biosensor applications. Normally, enzymes are surrounding by thick layer of insulating protein, so the electrons produced from the reaction were difficult to transfer to electrode surface. The conductive materials, mostly metal nanoparticles at nanoscales were applied for electron transfer improvement between electrodes and enzyme active centers.

2.2 Carbon nanotube

Carbon nanotubes are the basic building blocks of nanotechnology. Carbon nanotube have tensile strength equal to one hundred time of steel, better thermal conductivity compared to diamond. Carbon nanotube have better electrical conductivity similar to copper but more capable to carry higher currents. All this unique properties make carbon nanotubes as a wonder material [94].

2.2.1 Types of carbon nanotubes

Carbon nanotubes can exist in variety of shape; single wall, multi wall, long, short, open and closed. A different type of carbon nanotubes were discuss in below paragraph:

2.2.1.1 Single-wall carbon nanotube

Single-wall carbon nanotube (SWCN) have diameter close to 1 nanometer with a tube length that can reach millions times longer. Average diameters estimated 1.2 nanometer, depend on the synthesis methods. The structure of single wall carbon nanotube is like wrapping a one atom thick layer of graphite called grapheme into a seamless cylinder. SWCNs are more flexible than multiwall carbon nanotubes because it can be twisted flattened and bent into small circles without breaking. Carbon nanotubes have electrical properties like a metal or semiconducting, by adjusting the electrical field.

2.2.1.2 Multi-walled carbon nanotube

Multi-walled carbon nanotube (MWNT) consists a number of SWNTs and complex structures. The typical size for MWNTs is 100 times longer and has outer diameters in 10 nanometers. There are variety shapes of MWNT such as like bamboo-trunks, sea urchins, necklaces or coils [95]. MWNT have wide application because they are easier to produce in large quantities at a reasonable price. 2 models are applied to describe the structure of multi-walled carbon nanotube. If the sheet of graphite are arranged in cylinders, it is called Russian Doll model. If single sheet of graphite is rolled in around itself like rolled newspaper, it is called Parchment model.

2.2.1.3 Carbon nanohorns

Carbon nanohorns was first published by Harris et al and lijima et.al. [96]. The morphology of single walled carbon nanohorns (SWCNHs) are horn-shaped single-walled tubules with a conical tip. The advantages for this type of carbon nanotube are no catalysis is required during synthesis process. Therefore, high purity materials can be produced. Their unique properties such as high surface area and good electronic properties make them as a good candidate for energy storage [97]. Carbon nanohorns have been widely applied in various applications, such as gas storage, adsorption, catalyst support, and fuel cells [98].

2.2.2 Methods to synthesize carbon nanotubes

There are a few techniques that already been used to synthesized the carbon nanotubes. Below paragraph is the example of the techniques to synthesized carbon nanotubes.

2.2.2.1 Arc evaporation method

This method produces high quality of carbon nanotubes. The process involves passing a current 50 ampere between 2 graphite electrodes in helium atmosphere as show in Figure 2.4 [99]. This will causes graphite to vaporize and condense at reaction vessel wall and cathode. The condense graphite at cathode contains carbon nanotubes. In 1950, carbon nanotube can be synthesized by using carbon containing gas passing process. Usually this reaction will used small size of metal particles catalyst such as Fe, Co or Ni. This catalyst will breakdown the gaseous molecule to carbon and it will grow with metal particle at the tip [100, 101]. The tube that produced by arc discharge evaoratin method is similar to fullerene synthesis. The dimension of carbon ranging from 4 to 30 nm in diameter and up to 1 mm in length. Iijima published a paper in 1991 mentioned about new structure of carbon consisting of needle-like tubes.

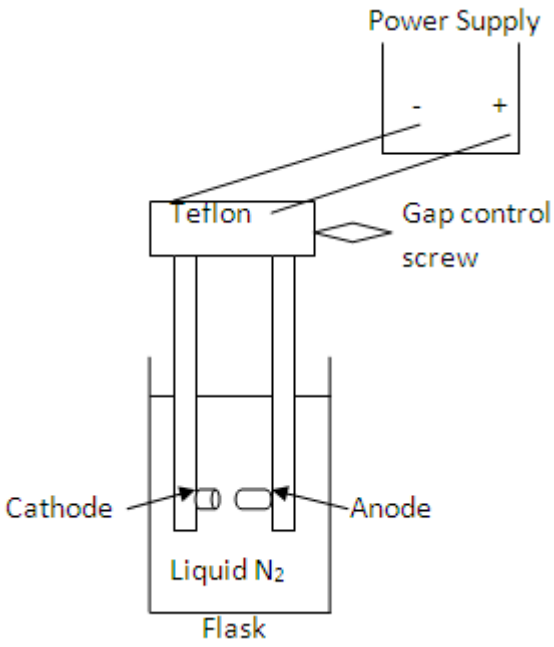

Figure 2. 4 Experimental arc discharge set-up in liquid N_2.

2.2.2.2 Chemical vapor deposition (CVD)

Chemical vapor deposition is the catalytic decomposition of hydrocarbon or carbon monoxide feedstock with help of metal catalyst. Carbon source is then placed in gas phase in reaction chamber as show in Figure 2.5 [102]. After that carbon molecule is converted to atomic level by using energy source like heated coil. The atomic carbon then diffuse on substrate, after coated with catalyst, and the growth tube can be observed over the catalyst. Methane, carbon monoxide or acetylene was use as carbon source with heating temperature range from 650 – 900ºC. The morphology of carbon nanotubes produced by this process depend on temperature and the operation pressure, the type, volume and concentration of hydrocarbon, the nature, size and the pretreatment of metallic catalyst, the nature of the support and the reaction time [102].

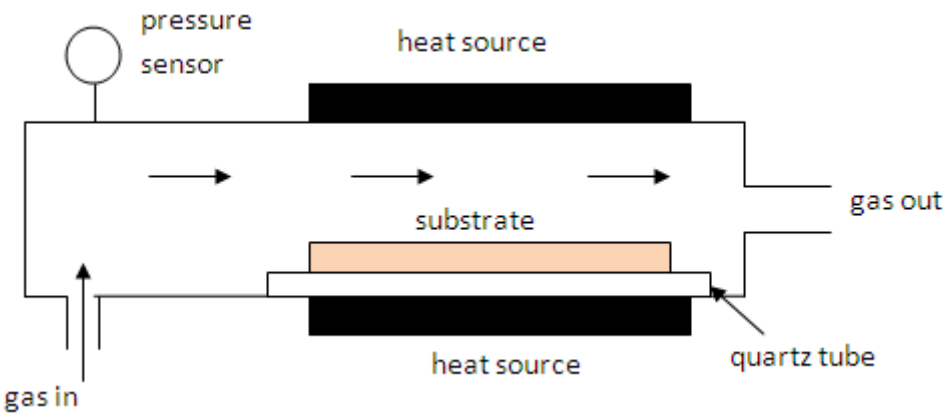

Figure 2. 5 Schematic demonstration of CVD method of horizontal furnace

2.2.2.3 Hydrothermal method

This method has been successfully synthesized variety of carbon nanotubes such as nano-onions, nanorods, nanowires, nanobelts, MWNTs. A mixture of polyethylene and water with a Ni catalyst were used to produced several to more than 100 carbon layers of MWNTs by using this method [103]. Graphitic carbon nanotubes were synthesized by the same research group using ethylene glycol ($C_2H_4O_2$) solution in the presence of Ni catalyst [104] typically, hydrothermal nanotubes have wall thickness of 7–25 nm and outer diameter of 50–150 nm. Thin-wall carbon tubes with internal diameters from 10 to 1000 nm have been also produce.

Carbon nanotubes can be prepared in large quantity by using sonochemical/hydrothermal method [105]. have prepared large quantity of carbon nanotubes using sonochemical/hydrothermal method. Manafi et al. used 5 mol/l NaOH aqueous solutions of dichloromethane, $CoCl_2$ and metallic Li as a starting materials. The synthesis condition such as heating temperature and time that had been used for this process are 150–160 °C for 24 h.

The nanotubes sizes that produced in this process about 60 nm in diameter and 2–5 μm long. This method also used to growth multiwall carbon nanocells and multiwall carbon nanotubes from amorphous carbon, at temperatures below 800 °C [105]. Diameters for nanocells are smaller than 100 nm. The nanotubes produced in the sample range of tens for diameters and hundreds of nanometers for length [106]. Table 2.2 summarizes about advantages and disadvantages for each methods for synthesize carbon nanotubes.

Table 2 .2 Advantages and disadvantages of methods for carbon nanotube synthesis

Method	Advantage	Disadvantage
Arc Evaporation	Can be scaled up for volume production	Quality of carbon is poorer
Chemical Vapor Deposition	• high growth rates possible • can deposit materials which are hard to evaporate • good reproducibility	• high temperatures • complex processes • toxic and corrosive gasses
Hydrothermal	No hydrocarbon or carrier gas are required	high cost of equipment and the inability to monitor crystals in the process of their growth

2.2.3 Properties of carbon nanotubes

The unique properties of carbon nanotubes such as stiffness, strength compared to other fiber materials, which normally lack from the mentioned properties. Below is summarizing for carbon nanotubes properties:

2.2.3.1 Mechanical properties

Carbon nanotubes can be categorized as strongest materials. This properties attributed from covalent sp^3 bonds formed between the individual carbon atoms [94]. Carbon nanotubes are extremely strong because of C-C bonds and have high Young's modulus estimated is 1 Tpa to 1.8 Tpa [94]. The modulus of a SWNT depends on the diameter and chirality. For multi-walled carbon nanotubes, the outer graphitic shell only can support stress when tubes are dispersed in epoxy matrix. For single wall nanotube have weak inter tube cohension due to shearing effects [107]. A perfect nanotube has strength about 10 to 100 times than steel per unit weight. The Young's modulus of perfect nanotubes can reach as high as 1000 GPa. The tensile strength of nanotubes can reach up to 63 GPa, 50 times higher than steel.

2.2.3.2 Electrical properties

Carbon nanotubes have unique electrical properties. A single graphite sheet has properties of intermediate between semiconductors and metals. Theoretically, metallic nanotubes can conduct electrical current of 4×10^9 A/cm^2 which is higher 1,000 times than copper [108]. The defect and lattice vibration will affect electrical transport of carbon nanotubes.

2.2.3.3 Thermal properties

Nanotubes expected to have very good thermal conductors, possesses "ballistic conduction," properties but also good insulators. The carbon nanotube will be able to transmit up to 6000 $W \cdot m^{-1} \cdot K^{-1}$ at room temperature; compare to copper which transmits 385 $W \cdot m^{-1} \cdot K^{-1}$. Carbon nanotubes are stable at temperature up to 2800 °C in vacuum and about 750 °C in air.

2.3 Introduction of crystallization

Crystallization of substances from supersaturated solutions at normal pressure conditions in suitable nonreactive solvents in which they are fairly soluble is usually referred to as crystal growth from solutions. The solvents used for the crystallization of different substances are usually water and various organic liquid and their mixtures, and melts of some chemical compounds and their mixtures. For crystal growth at low temperature solution, the crystallization temperatures generally do not exceed 70-80 ^{o}C. For crystal growth at high temperature solution, the crystallization temperatures rarely exceed 1200-1300 ^{o}C [109].

Crystal growth from low temperature is usually to growth a single crystals when the starting materials are not stable at high temperature. It also allows crystals of the same substance to grow in a variety of morphologies and polymorphic forms by variations of growth conditions or of the solvent. The produced materials ranging from micrometer sized crystalline to large sized are growth from low temperature solutions. The method is widely used because

1) The growth apparatus is relatively simple and cheap

2) introduces small thermal stresses in the crystals

3) The crystal obtained usually have well-developed face.

For high temperature solution growth, the metal catalyst dissolved in solvent before crystallization process. The solution must be supersaturated before crystallization process take place. The supersaturation occurs by evaporation the solvent. There are 2 types of high temperature crystal growth:

1. Growth from single component system.

2. Growth from multi component system.

The high temperature crystal growth has been widely used to growth crystals oxide. The process begin with heating the container and solution to the temperature that allowed all solute materials to dissolve.

2.3.1 Crystal growth techniques

Crystal growth methods differ in the way the supersaturation is generated and maintained constant during a growth run, and 3D nucleation is initiated. In general, temperature coefficient of its solubility is the parameter that need to be consider in selection the method to growth the compound. If the compound has their own temperature coefficient of solubility, the crystal can be grown by changing the temperature (temperature changing method). In principle, substance with both positive (+ deg) as well as negative temperature (- deg) coefficients of solubility can be grown by this technique. At particular temperature, if the compound transform the phase transition, the above methods cannot be used. When the solubility remains practically constant with a change in temperature, the supersaturation can be created by evaporating the solvent (solvent evaporation method).

For solvent evaporation technique, the super saturation required to growth the crystal by evaporating solvent at a constant temperature. Excess mass of the substance for crystallization is created from a consideration of the solubility of the compound in the solvent and the evaporation rate of the solvent. In most cases, the pressure of the solvent vapor over the solutions is higher than that of the solute. This enables one to evaporate solvent vapor into the atmosphere or withdraw it as

condensate using water-cooled coils. Therefore, the supersaturation necessary for crystal growth can be maintained by controlled evaporation of the solvent. The mass of the deposited substance Δm is proportional to the volume ΔV of the solvent removed from the solution and to the concentration c of the substance in the solution. Therefore, crystal growth rate is controlled by changing the rate of evaporation of the solvent. Table 2.3 discusses about advantages and disadvantages for different method of crystallization process.

Table 2. 3 Advantages and disadvantages for crystallization methods

Method	Advantages	Disadvantages
Gel growth (low temp crystal growth)	Growth process can be done at room temperature (20 – 40 ^{0}C)	Crystal growth take about 3 – 4 weeks
Hydrothermal growth (middle temp crystal growth)	Suitable for growth of large good-quality crystal while maintaining control over composition	Difficult to observe crystal growth
Bridgman technique (high temp crystal growth)	Raw materials are sealed in crucible, reduce the volatilization by leakage and pollution	1) Difficult to observe crystal growth 2) seed crystals required
Chemical Vapour Transport technique (CVT) (high temp crystal growth)	Good method for growing high quality crystals from powders	Transporting agent may incorporated as impurities in growth process

2.4 Biosensor

Biosensor development started in 1962 by Leland C Clark Jr., who is known as the father of biosensors. Biosensor consists of 2 main parts which are 1) biomolecule such as enzyme, antibody or nucleic acid, 2) transducer that converts the signal, which can be electron transfer, optical or thermal change, into a measureable electrical parameter such as current or voltages. Biosensors can be classified as shows in Figure 2.6. Biosensors have many uses in clinical analysis, general health care monitoring, industrial processing and monitoring, and environmental pollution control.

Biosensor has very important roles in application which requires selective measurement. Biosensor will react with specific analyte of substrate by the highly specific biological component. The first biosensor was built in 1962 by Clark. This biosensor was used to determine glucose in blood samples. Then in 1967, Updika and Hicks entrapped glucose oxidase enzyme in a polyacrylamide gel to increase stability of the enzyme electrode. Since then, a lots of researchers try to stabilize the enzymes electrode by using polymer, cell and organelles. Biosensor can be divided into various categories. For this work, electrochemical biosensor will be used for the H_2O_2 detection. Electrochemical biosensor offers very good properties compared with other types of biosensor technique. Under the electrochemical biosensor, there are 3 methods, amperometry, potentiometry and conductimetry.

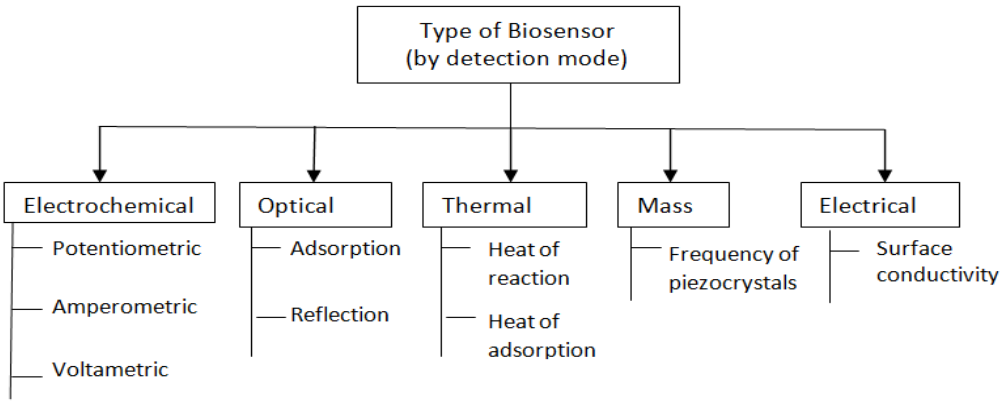

Figure 2. 6 Type of biosensors based on detection mode

2.4.1 Biosensor Characterizations

Biosensor can be characterized according to below factors:

2.4.1.1 Dynamic range and sensitivity

Sensor calibration is normally performed by adding standard solution of the analyte and plotting the response minus by background signal, versus the analyte concentration or its logarithm. Sensitivity is to be determined within the dynamic range, which is the linear concentration range of the calibration curve.

2.4.1.2 Selectivity

Selectivity properties is related to biological receptor and transducer. Naturally, bacteria, yeast or tissue cultures are not specific. But most of the enzymes are specific such as peroxidase, laccase, tyrosinase, and ceruloplasmin. This enzymes are used for selective biosensors fabrication.

2.4.1.3 Reproducibility and reliability

Reproducibility is measuring a series of data over a period of time. This testing will determined analyte concentration in the dynamic range. The reliability of a biosensor depends on both its selectivity and reproducibility. These properties will determine under present of interfering substances under actual operating condition.

2.4.1.4 Response time

The time required to reach 90% of the response. The response time depends on the analyte and the activity of the enzyme.

2.4.1.5 Stability

The stability of a biosensor may vary depend on the sensor geometry, applied enzyme or transducer, method of preparation.

2.5 Hydrogen peroxide

H_2O_2 is a colorless liquid, slightly more viscous than water (density = 1.1 g/ml, giving a molarity of 9.8 M) and completely miscible in water and alcohol. It behaves as a weak acid (pKa = 11.6) and at alkaline pH's it deprotonates to form a perhydroxyl ion along with a hydrogen ion [110].

$$H_2O_2 \leftrightarrow H^+ + HO_2^- \quad (5)$$

H_2O_2 is unstable and it decomposes to oxygen and water. It will rapidly decompose when catalysis agents (like iron) are present. The reaction corresponding to the decomposition of H_2O_2 is as follow [110]:

$$2H_2O_2 \rightarrow O_2 + 2H_2O \quad (6)$$

H_2O_2 is considered a strong oxidizing agent, but is dependent on the pH. The half-cell reaction for H_2O_2 in acidic and neutral aqueous solution is as follow [110]:

Acid & Neutral $H_2O_2 + 2H^+ + 2e^- \rightarrow 2H_2O$ (7)

The standard potential for reaction (7) is 1.76 V, so H_2O_2 behaves as a powerful oxidizing agent in acid solutions. In basic solutions, however, the half-cell potential is lower (E_0 = 0.87 V) because of the presence of the perhydroxyl ion rather than of the H_2O_2 molecule [110]:

Base $HO_2^- + H_2O + 2e^- \rightarrow 3OH^-$ (8)

H_2O_2 can also behave as a reducing agent. The half-cell reaction in acidic solution is as follow [110]:

Acid $H_2O_2 \rightarrow 2H^+ + O_2 + 2e^-$ (9)

The standard potential for reaction (9) is -0.69 V. The corresponding half-cell reaction in basic conditions has a standard potential of -0.08 V and is [110]:

Base $HO_2^- + OH^- \rightarrow O_2 + H_2O + 2e^-$ (10)

Generally, electrochemical reactions of H_2O_2 present slow electrode kinetics on many electrode materials and as a result, high potentials are required. Therefore catalysts are needed to lower the potential during electrochemical oxidation and reduction of H_2O_2.

2.5.1 Method for hydrogen peroxide detection

There are numerous techniques to detect hydrogen peroxide that already been published in literature. The methods for the determination of H_2O_2 concentration can be divided into five categories: titrimetry, spectrophotometry, fluorescence, chemiluminescence and electrochemical methods as explain in below paragraph:

2.5.1.1 Titration method

There are several titration methods to detect H_2O_2, for example iodometric method. The iodometric method is widely used in 1880 after being introduced by Kingzett [111]. This method will oxidize the iodide to iodine using H_2O_2 in the presence of molybdate as a catalyst. The subsequent titration of the iodine formed with a thiosulfate solution using a starch indicator to indicate the end point.

$H_2O_2 + 2\ KI + H_2SO_4 \rightarrow I_2 + K_2SO_4 + 2\ H_2O$ (11)

2.5.1.2 Spectrophotometric

Matsubara et al. [112] used a water-soluble titanium (IV)-porpyrin complex, [$TiO(tpypH_4)^{4+}$] to determine trace amounts of H_2O_2. It was observed that the absorbance of $TiO(typyH_4)^{4+}$ at 432 nm due to the consumption of $TiO(tpypH_4)^{4+}$ accompanied by the formation of $TiO_2(trypH_4)^{4+}$. This reagent was used for the determination of H_2O_2 in water samples such as tap water and rainwater and absorbance was found to be proportional to H_2O_2 concentration in the range 1.0×10^{-8} to 2.8×10^{-6} M.

2.5.1.3 Fluorescence method

Horseradish peroxidase (HRP) is a heme-containing enzyme and the most commonly used enzyme in H_2O_2 determination due to its high selectivity. Chang et al. [113] developed a sensing probe for H_2O_2 based on the HRP immobilization on Fe_3O_4/SiO_2 magnetic nanoparticles. H_2O_2 was activated in the presence of HRP and oxidized non-fluorescent 3-(4-hydroxyphenyl)propionic acid (HPPA) to a fluorescent product with an emission maximum at 409 nm.

2.5.1.4 Chemiluminescence

When H_2O_2 is mixed with luminol in the presence of a catalyst, the decomposition of H_2O_2 leads to a sequence of reactions resulting in the release of photons from a luminol byproduct. Hanaoko et al. reported the determination of H_2O_2 by chemiluminescence (CL), using a heterogeneous catalyst, Co(II)-monoethanolamine complex immobilized on Dowex-50W resin [113]. They developed a H_2O_2 flow sensor, which showed a linear ratio of CL versus the concentration of H_2O_2 in the range $2x10^{-7}$ to 2×10^{-5} M and a detection limit of $1x10^{-7}$ M (S/N=3).

2.5.1.5 Amperometric sensor

Amperometric sensor is based on the measurement of the current resulting from the electrochemical oxidation or reduction of an electroactive species. The output signal was obtained by applying potential at the working electrode and monitoring the current as a function of time. The applied potential provides the driving force for the electron transfer reaction. The relationship between the moles, N, of electroactive species reacted and the charge passed through the sensor, Q, is known as Faraday's Law:

$$N = Q/nF \qquad (12)$$

where n is the number of electrons transferred and F is the Faraday constant (F= 96487 /mol)

2.5.1.6 Potentiometric sensors

Potentiometric measurements rely on the determination of the potential difference at zero current. The analytical information is obtained by converting the recognition process into a potential difference, which is proportional to the concentration of targeted species generated or consumed. The relationship between the potential and the ionic concentration in solution in a potentiometric chemical sensor is given by the Nernst equation:

$$\mathrm{E} = \mathrm{E_o}\text{-}\frac{0.05916\mathrm{V}}{\mathrm{z}}\log 10\,\frac{\mathrm{a_{Red}}}{\mathrm{a_{Ox}}} \qquad (13)$$

Where E is the cell potential, E_0 is the standard cell potential, z is the number of moles of electrons transferred in the cell reaction, and a $_{Red}$ and a $_{Ox}$ are the chemical

activities for the reductant and oxidant species, respectively. Table 2.4 show the advantage and disadvantage for different methods for hydrogen peroxide detection.

Table 2. 4 Advantages and disadvantages of different method for hydrogen peroxide detection

Method	Advantage	Disadvantage
Titration	Requires a low-skill and train operators	Catalysis or interference from transition metal may effect the accuracy of the measurement
Spectrophotometric	Modification method can detect low quantities of the compound	Possible interfering agents included transitions metal and oxidants such as chlorine
Fluorescence	Fairly sensitive and thus can detect low quantities of the compound	It requires expensive and sophisticated equipment
Chemiluminescence	Can detect a wide variety of sampling substances such as dilute solution, concentrated salution, suspension, flowing liquids and solid surfaces.	Time consuming and highly prone to interferences
Electrochemical	Inexpensive and high sensitivity method	Requires suitable potential to avoid any interferences during measurement

2.5.2 Materials for H_2O_2 detection

The main objective to build a sensor is to get high degree of the selectivity toward the analyte. There are some factors that affect the selectivity such as suitable electrical potential, introducing the catalyst and modified with selective membranes. Many materials have been used for hydrogen peroxide detection. This section will give information about materials that had been used to detect hydrogen peroxide. Example of materials that had been used to detect the hydrogen peroxide as listed below:

2.5.2.1 Platinum

In the past, platinum is the popular material for hydrogen peroxide detection. For example, Zhang et al. [114] used Pt disk electrodes to fabricate electrochemical for hydrogen peroxide detection. Amperometric testing was conducted at potential 0.65 V. The results are strongly dependent with pH, temperature and surface conditioning. Hall et al. [115] also used Pt rotating disk electrode to fabricate electrochemical hydrogen peroxide sensor by varying the concentration and rotation rates. Wang et al. [116] did some modification on Pt electrode by using a polyaniline and single-walled carbon nanotubes. However, Pt electrode is expensive and susceptible to poisoning, so require meticulous cleaning pretreatment procedures.

2.5.2.2 Other metals and metal alloys

Other materials that can be considered to replace Pt are Fe, Zn, Cu, Pd and metal alloys such as Pd/Au, Pd/If and Au/Pt had been used as a catalyst for hydrogen peroxide detection. Zen et al. [117] developed a disposable copper-plated screen printed carbon electrode (Cu SPE) for hydrogen peroxide detection at ambient

temperature. The detection of hydrogen peroxide was performed at potential -0.3 V with a sensitivity of 3.45 x 10^{-2} M. Kumar and Sornambikai [118] fabricated Nafion/Cu modified glassy carbon electrode. The electrochemical testing was carried out by applying - 0.2 V and successfully detect hydrogen peroxide in milk, human urine and green tea. Pd, Ru and Pd-Ru nanoparticles have been also investigated as electrocatalysts for H_2O_2.

2.5.2.3 Protein and enzyme-based sensors

Other than metal, biological component also had been used in hydrogen peroxide detection. There are many biological components with redox protein such as hemoglobin, soybean peroxidase, myoglobin and horseradish peroxidase (HRP). Among all this biological component, enzymes is the most common to use because of its high purity and low cost. There are so many methods to immobilize the enzymes on the electrodes surface such as adsorption, cross-linking and polymer entrapment. Yemini [119] fabricated HRP modified gold electrode by using horseradish peroxidase and peptide. Li et al. [120] studied about amperometric biosensor where HRP was immobilized on a sandwiched nano-Au particle/ m-phenylenediamine polymer film by glutaraldehyde cross-linking. The sensor presented a detection limit of 1.3 x 10^{-7} M and was used to determine H_2O_2 concentration in plant leaf sample.

2.6 Materials characterization methods

2.6.1 Brunauer–Emmett–Teller (BET)

Brunauer–Emmett–Teller (BET) theory explained about physical adsorption of gas molecules on a solid surface and to measure specific surface area of a material. The BET theory refers to multilayer adsorption as shown in Figure 2.7. Usually adopts non-corrosive gases (like nitrogen, argon, carbon dioxide, etc.) as adsorbates to determine the surface area data. Figure 2.8 showed standard BET graph where x-axis is the relative pressure and y axis is adsorption gas [121].

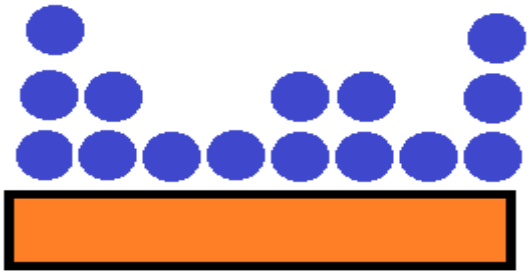

Figure 2. 7 BET model of multilayer adsorption, covered by one, two, three layer of adsorbate molecules.

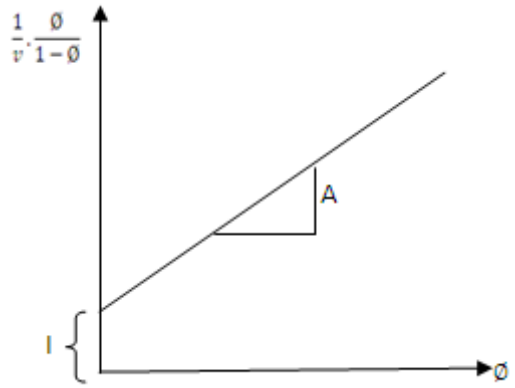

Figure 2. 8 BET plot

The Brunaeur, Emmett and Teller (BET) adsorption isotherm equation as follows:

$$\frac{1}{v\left[\left(\frac{p_o}{p}\right)-1\right]} = \frac{c-1}{v_m c}\left(\frac{p}{p_o}\right) + \frac{1}{v_m c} \quad (14)$$

where p and p_0 is the equilibrium and the saturation pressure of adsorbates at the temperature of adsorption, v is the adsorbed gas quantity (volume units), and v_m is the monolayer adsorbed gas quantity. c is the BET constant,

$$c = exp\left(\frac{E_1 - E_L}{RT}\right) \quad (15)$$

where E_1 is the heat of adsorption for the first layer, and E_L is that for the second and higher layers and is equal to the heat of liquefaction.

Equation 15 is an adsorption isotherm and can be plotted as a straight line with 1/(v [(p_0 /p) – 1]) on the y-axis and φ = p / p_0 on the x-axis. This plot is called a BET plot.

The total surface area S_{total} and the specific surface area S_{BET} can be calculate by :

$$S_{total} = \frac{(v_m N s)}{V} \quad (16)$$

$$S_{BET} = \frac{S_{total}}{a} \quad (17)$$

where v_m is in units of volume which are also the units of the molar volume of the adsorbate gas, N is Avogadro's number, s the adsorption cross section of the adsorbing species, V the molar volume of the adsorbate gas, and a the mass of the solid sample or adsorbent.

2.6.2 X-Ray Diffraction (XRD)

To determine the structure of a crystal and position of atom in the lattice, the X-rays beam is directed at the crystal and the angles at which beam is diffracted are measured. Each diffracted X-ray signal corresponds to coherent reflection, called Bragg reflection. This reflection can be represented as Bragg's Law:

$$2d\ sin\theta = n\lambda \quad (18)$$

where λ is the wavelength of the rays, θ is the angle between the incident rays and the surface of crystal, d is the spacing between layers of atoms and n is a positive integer.

The analysis of XRD data includes qualitative (phase identification) and quantitative (lattice parameter determination and phase fraction analysis). The peak position will present the data of crystal system, space group symmetry, translational symmetry, unit cell dimension and qualitative phase identification. The peak intensities display information about unit cell contents, point symmetry and quantitative phase identification. The analysis of peak shape and width (full-width at half maximum) of the Bragg peaks of the X-ray diffraction pattern give information about crystal size and strain. The crystal size can be obtained by using Scherrer equation:

$$D_v = \frac{K\lambda}{B\cos\theta} \quad (19)$$

where D_v is volume weighted crystallite size, K is Scherrer constant, λ is wavelength of radiation, β is full-width at half maximum at 2θ

2.6.3 Transmission Electron Microscope (TEM)

In TEM, very high energy of electron beam is subjected to ultra-thin sample. An image is formed resulting from interaction between transmit electrons and sample. The image produce can be adjusted by focusing using the fluorescent screen. TEMs are capable to produced higher resolution image than light microscope. For this reason, most of nanomaterials are characterized using TEM machine. Crystal structure also can be investigated using phase contrast mode. The main problem before using the TEM machine is to make sure that the sample is conductive. Special coating is required for insulating materials before subjecting to TEM testing.

2.6.4 Fourier Transforms Infrared spectroscopy (FTIR)

In FTIR testing, the infrared radiations were passing through a sample. Some of the infrared radiations were absorbed by sample and some of it is passed through (transmitted). The spectrum display information about molecular absorption and transmission as a fingerprint of the sample. FTIR was used to identify unknown materials, quality or consistency of a sample and amount of components in a mixture. The FTIR spectrum resulting from vibration frequency between the bonds of the materials. Every materials have their unique properties, so FTIR spectrum cannot be duplicate. Therefore FTIR spectrum can be used to identify different kind of materials. The size of the peaks is represent amount of materials present. Simple layout for FTIR spectrum is show in Figure 2.9.

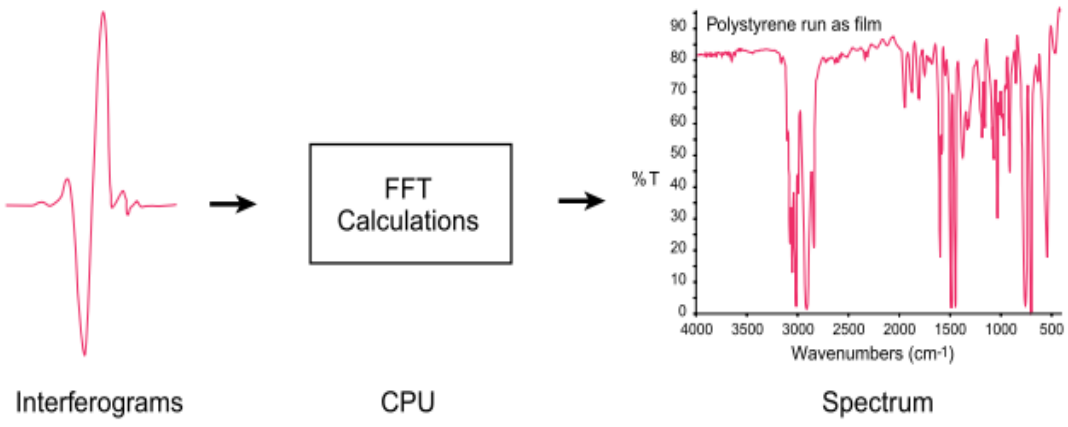

Figure 2. 9 Simple spectrometer layout

2.6.5 Raman spectroscopy

Raman is the technique that required to collect the spectrum, so the sample will placed at excitation beam and scattered light were collected. For Raman spectrum, there is no 2 molecules give exactly the same Raman Spectrum. The intensity of scattered light is proportional to amount of material present. Therefore, Raman provides both quantitative and qualitative of the sample. This testing is non - destructive testing. No special treatment or modification of the sample are required. This advantages make Raman testing is suitable for physical properties study such as crystallinity, phase transitions and polymorphs. Figure 2.10 show Raman Spectra processing step. An interferometer converts the Raman signal into an interferogram. The entire spectrum was deliver onto detector. Application of the Fourier transform algorithm to the interferogram converts the results into a conventional Raman spectrum.

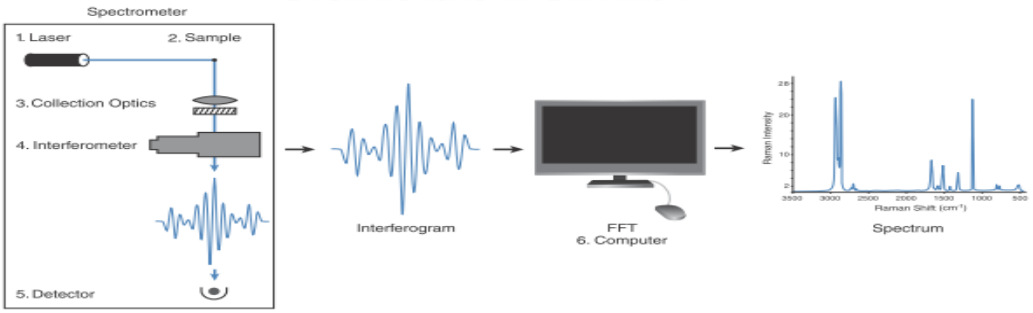

Figure 2. 10 Raman Spectrum

2.6.6 Cyclic voltammetry

Cyclic voltanmmetry give the information about current obtained when the potential is varied. From cyclic voltammetry result, we can determine thermodynamics of redox processes, kinetics of heterogeneous electron transfer reaction and adsorption processes

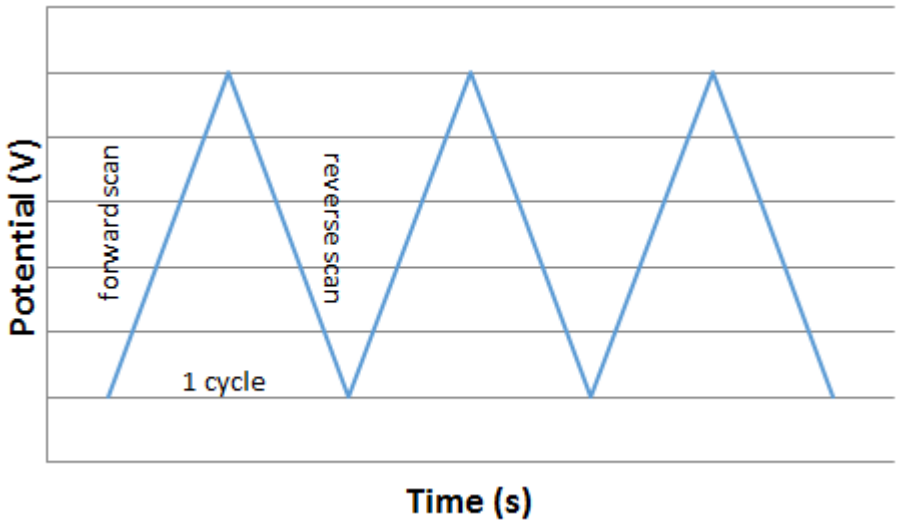

Figure 2. 11 Potential time excitation signal in cyclic voltammogram

Cyclic voltammetry consists of linear scanning of the potential of working electrode using a triangular potential waveform as shown in Figure 2.11. The resulting plot of current versus potential is referred as a cyclic voltammogram. Figure 2.12 shows redox reaction in cyclic voltammogram

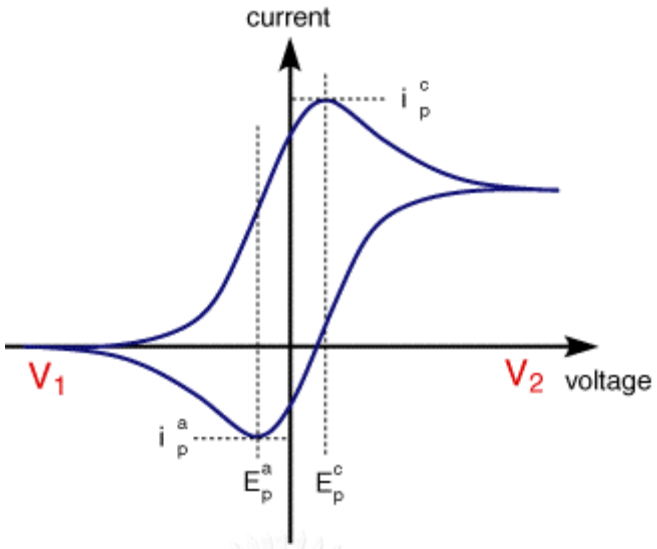

Figure 2. 12 Redox reaction in cyclic voltammogram

For reversible systems, the peak current at 25°C is given by Randless-Sevcik equation:

$$i_p = (2.69\ x\ 10^5)n^{3/2}ACD^{1/2}v^{1/2} \quad (20)$$

where n is the number of electron involved in the reaction. A is electrode area (cm^2), C is the concentration (mol cm^{-3}), D is diffusion coefficient of species and v is the scan rate (V s^{-1}). The position of the peaks on the potential axis (E_p) is related to the standard potential of the redox process. The standard potential for a reversible couple is between $E_{p.a}$ and $E_{p,c}$

$$E_o = \frac{E_{p,a}+E_{p,c}}{2} \quad (21)$$

The separation between the peak potentials is given:

$$\Delta E_p = E_{p,a} - E_{p,c} = \frac{0.059\ V}{n} \quad (22)$$

The peak separation can be used to determine the number of electrons transferred followingernst behavior.

2.6.7 Amperometry

Amperometry is measurement based on resulting current from reduction and oxidation of electroactive species. The signal that generated on transducer is resulting from potential at the working electrode. The current produced is monitoring with a time. The applied potential provides the driving force for electron transfer on the transducer [122]. The resulting current is directly proportional to the rate of electron transfer reaction. The current of reaction by the complete current-potential characteristic can be represent as followed: [123, 124]:

$$i = nFAk^0\left[C_0 e^{-\alpha nF(E-E^0)/RT} - C_R e^{(1-\alpha)nF(E-E^0)/RT}\right] \qquad (23)$$

where i is the current, F is Faraday's constant, A is electrode area, C is the concentration of the species, n is number of electron involve in the reaction, α is asymmetrical constant, x is the distance and E is the potential.

Chapter 3
Methodology

This section will discuss about experimental design for synthesize carbon nanotubes and transition metals oxide. After synthesize the nanoparticles, the materials characterization testing were carried out by using Transmission electron microscopy (TEM), Fourier transforms infrared spectroscopy (FTIR), Raman spectroscopy, Brunauer–Emmett–Teller (BET) and X-ray diffraction. The method for sensors fabrication also will include in this section. Electrochemical techniques were used to characterize the fabricated sensors.

3.1 Chemical and reagents

All chemicals were analytical grade reagents and used as received without further purification. NiO and MnO were synthesized from $Ni(CH_3COO)_2.4H_2O$ (99%), $KMnO_4$ (98%) and $Mn(CH_3COO)_2.4H_2O$ (98%). Glycerol (99.5%) and ferrocene (98%) and ethylene glycol were obtained from Aldrich and used as received. Hydrogen peroxide (30%) was from local supplier. All the solutions were prepared using deionized water. HRP (140 Umg^{-1}) was from Fluka Analytical and used without further purification. Dopamine hydrochloride was obtained from Sigma.

3.2 Apparatus

Figure 3.1 shows stainless steel bomb using for nickel oxides (NiO) and manganese oxide (MnO) synthesis. The mixture of compounds in alumina crucible was placed inside this stainless steel bomb to make sure that there is no outside factors that will involve during heating time. P-Series Muffle Furnace as shown in Figure. 3.2 were used to synthesize nickel oxide and manganese oxide. Electrochemical testing was carried out by using home-made potentiostat as shown in Figure 3.3. The commercial gold electrodes as shown in Figure 3.4 were used for electrochemical testing for this work. Carbon nanotune was synthesized using tube furnace.

The materials characterizations of the nanomaterials were performed using Brunaer-Emmett-Teller (BET), X-ray diffraction (XRD), transmission electron microscope (TEM). Raman spectroscopy and Fourier transform infrared spectroscopy (FTIR).

Figure 3. 1 stainless steel bomb

Figure 3. 2 Furnace for synthesizing NiO and MnO

Figure 3. 3 Home made potentiostat machine

Figure 3. 4 Commercial Gold Electrode

3.3 Synthesis of nickel oxide and manganese oxide

All experiments were conducted under air atmosphere. In preparing nickel oxide (NiO), $Ni(CH_3COO)_2.4H_2O$ were dissolved in H_2O and ethylene glycol as shown in Figure 3.5. The optimum studies were conducted to choose high surface area of nickel oxide by variying the concentration of the solvent (0.05 – 0.5 M), heating temperature (100 – 300^oC), heating time (3 – 7 hours) and types of solvents (ethylene glycol: water (1:1), water only). The mixture were transferred into bomb stainless steel as shown in Figure 3.6. The process flow chart of the nickel oxide as shown in Figure 3.7. The furnace was setting according to discussed parameters. The product was separated from the solution by filtration process as shown in Figure 3.8. Then the product was washed with deionized water and ethanol several times and finally dried at 120^oC in air. The powder further heated to 400^oC for 2 hours [124] . Finally, the black powder of NiO was obtained. Table 3.1 shows weight of nickel acetate precursor to synthesize nickel oxide.

Table 3. 1 Weight of nickel acetate precursor to synthesize nickel oxide

Concentration (M)	Nickel acetate (g)
0.05	0.260
0.1	0.521
0.3	1.562
0.5	2.600

In preparing manganese oxide (MnO), $Mn(CH_3COO)_2$ and $KMnO_4$ were individually dissolved in distilled water as shown in Figure 3.9. These solution were mixed together, with the molar ratio of $KMnO_4$ to $Mn(CH_3COO)_2$ = 1:1. The process flow chart of the manganese oxide is shown in Figure 3.10. The optimum study were conducted to choose high surface area of manganese oxide by varying the concentration of the solvent (0.05 – 0.5 M) and heating temperature (100 – 200 ^oC). The mixture solution was loaded into bomb stainless steel. During the hydrothermal reaction, the furnace was setting according to discussed parameters . The black precipitates were obtained and collected through filtration and washed with distilled water and finally dried at 120 ^oC for 10 hours [125]. Table 3.2 shows weight of manganese acetate and potassium permanganate precursors to synthesize manganese oxide

Table 3. 2 Weight of manganese acetate and potassium permanganate precursors to synthesize manganese oxide

Concentration (M)	Manganese(II) acetate (g)	Potassium permanganate (g)
0.05	0.245	0.158
0.1	0.490	0.316
0.3	1.470	0.948
0.5	2.450	1.580

Figure 3. 5 Mixture of Nickel acetate dilute with ethylene glycol and deionized water (1:1)

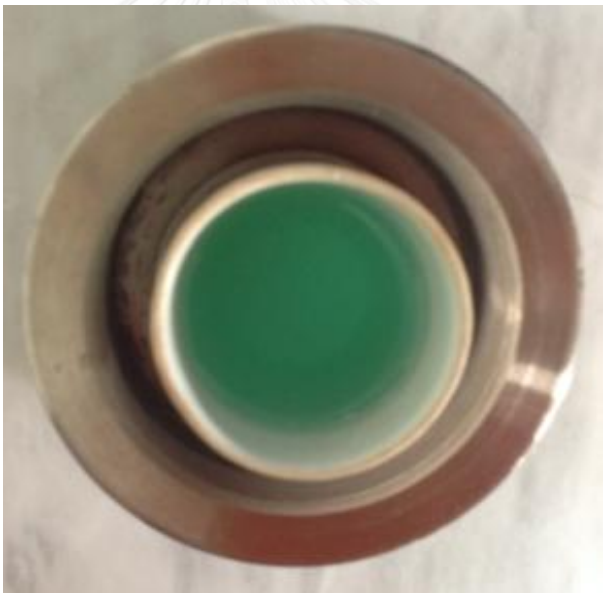

Figure 3. 6 Alumina crucibles in bomb stainless steel

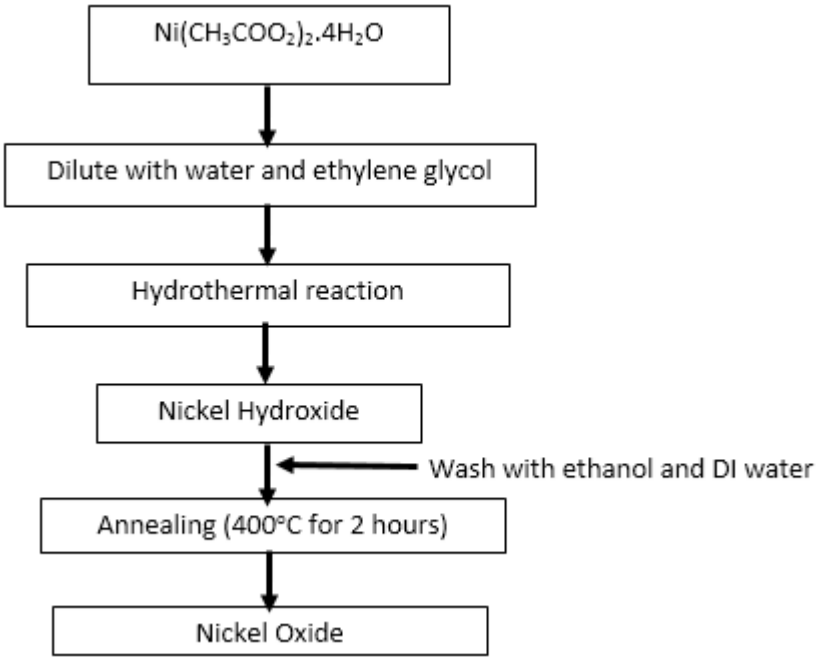

Figure 3. 7 Flow chart to synthesize nickel oxide

Figure 3. 8 Washing and filtering a nanomaterials

Figure 3. 9 Manganese acetate mix with potassium permanganate

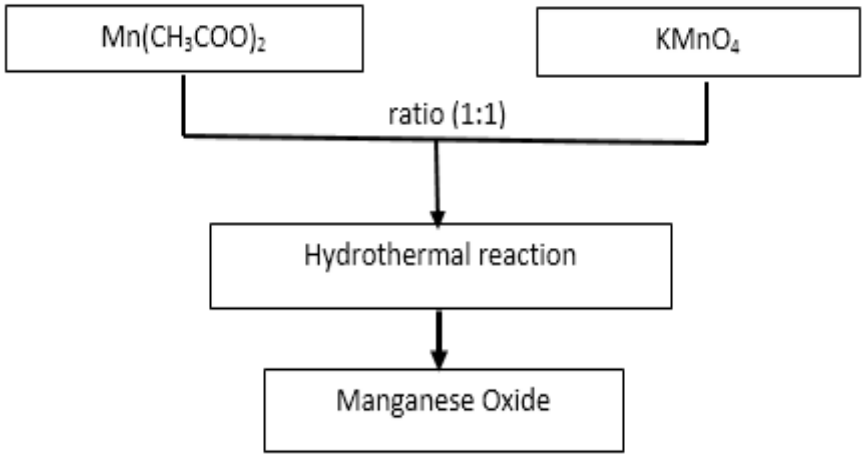

Figure 3. 10 Flow chart to synthesize manganese oxide

3.4 Synthesis of multi-walled carbon nanotubes

The multi-walled carbon nanotubes (MWCNTs) were prepared by chemical vapour deposition (CVD) technique. The process flow chart of the carbon nanotube is shown in Figure 3.11. The suspension was prepared by mixing glycerol and ferrocene with ratio 5:1 as show in Fig. 3.12. The suspension was transferred to the tube furnace and heat at 850^{o}C for 30 minutes as shown in Fig. 3.13. The nitrogen gas was flow to the tube furnace with the flow rate of 50 ml/min. The black powder was obtained at the end of the process as shown in Fig. 3.14. The carbon nanotubes were purified by washing with sulfuric acid and deionized water.

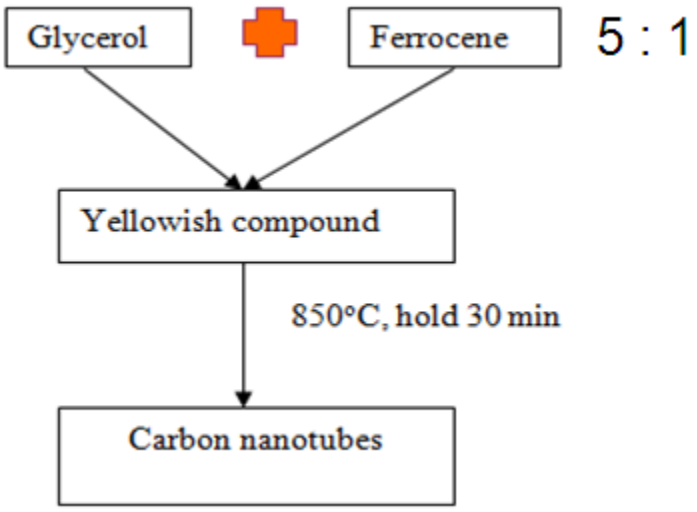

Figure 3. 11 Flow chart to synthesize carbon nanotube

Figure 3. 12 Mixture of glycerol and ferrocene

Figure 3. 13 Tube furnace

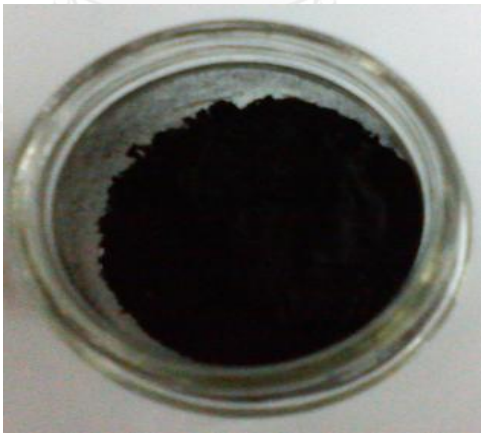

Figure 3. 14 Carbon nanotube

3.5 Materials characterizations

3.5.1 Brunauer–Emmett–Teller (BET)

The Brunauer–Emmett–Teller (BET) testing was conducted by using BELSORP mini-II model machine. The samples were weight and recorded. Before sending for BET testing, all samples must be heated for 2 hours. Figure 3.15 (a) and (b) shows heating machine and BET machine for study surface area of nanomaterials.

Figure 3. 15 (a) and (b) show heating machine and BET machine for study surface area of nanomaterials

3.5.2 X – Ray Diffraction (XRD)

The X –ray diffraction (XRD) testing was conducted by X- ray diffraction machine. The samples were smeared uniformly onto a glass slide. After that the glass slide was transferred to sample holder. Figure 3.16 shows the testing sample that was prepared on the glass slide and sample holder.

Figure 3. 16 Sample preparation for XRD testing

3.5.3 Transmission Electron Microscope (TEM)

The transmission electron microscope (TEM) testing was conducted by using JEM-3010-es model machine. A few amounts of nanomaterials was place on metal mesh grids. The sample grids were used as a material holder in TEM testing. Figure 3.17 shows (a) metal mesh grids and (b) TEM machine.

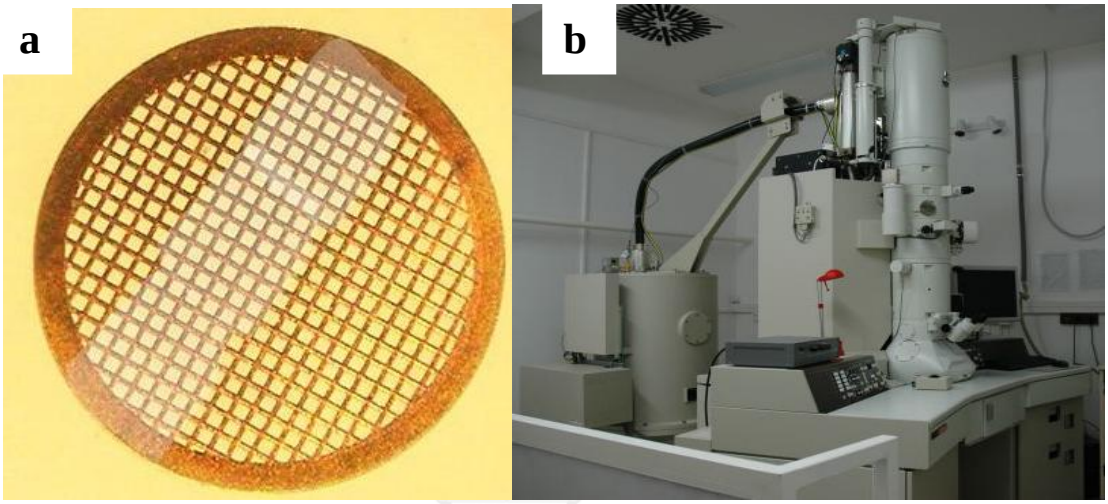

Figure 3. 17 (a) metal mesh grids; (b) transmission electron microscope machine.

3.5.4. Raman spectroscopy

The structures of nanomaterials were determined using Raman spectroscopy machine as shown in Fig 3.18. The testing samples were placed on the machine stainless stage. There is no sophisticated material preparation for Raman testing.

Figure 3. 18 Raman Spectroscopy Machine

3.5.5. Fourier Transforms Infrared spectroscopy (FTIR)

The Fourier transform infrared spectroscopy (FTIR) testing was conducted by using PerkinElmer model machine. A few amounts of nanomaterials was place on machine. FTIR is a non- destructive testing, so the sample can be used again for another testing.

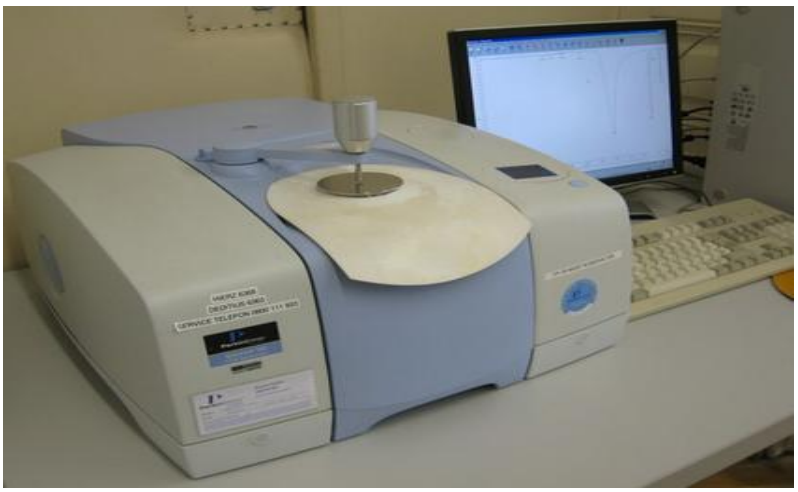

Figure 3. 19 FTIR Machine

3.6 Electrochemical testing

3.6.1 Preparation of single and binary catalyst electrodes

For single catalyst modified gold electrodes, dopamine solution was prepared by mixing 1 mg dopamine in 1 ml phosphate buffer (pH 8.4). Single catalyst solutions were individually prepared by mixing 1 mg of each nickel oxide and manganese oxide in 1 ml ethanol solution. Single catalyst modified electrodes were prepared by dropping 10 µl of single catalyst suspension on the electrodes surface and dried at room temperature (first layer). Then, 6 µl of dopamine solution was dropped onto metal oxide layer and dried at room temperature under exposure to the room light for 7 hours (second layer).

For binary catalyst modified gold electrode, 1 mg nickel oxide and 1 mg manganese oxide were mixed in 1 ml of ethanol solution. Then 10 µl of this suspension was dropped on the electrode surface and dried at room temperature (first layer). Then, 6 µl of dopamine solution was dropped onto metal oxide layer and dried at room temperature under exposed to the room light for 7 hours (second layer).

Schematic of modified electrode for amperometry testing is shown in Fig. 3.20.

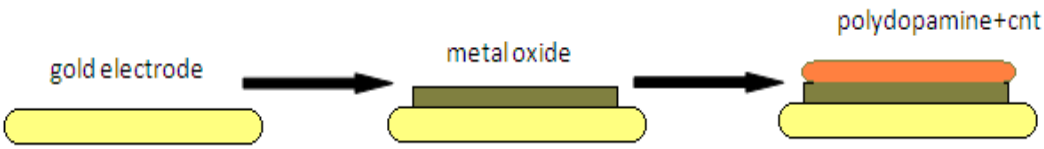

Figure 3. 20 layer-by-layer assembled films modified gold electrodes

3.6.2 Preparation of the enzyme electrode

To prepare modified gold electrode with horseradish peroxidase enzyme, 7% of glutaraldehyde was dropped on the electrode surface for 30 minutes. Glutaraldehyde acts as crosslinker between enzyme and modified electrode layer on the electrode surface. Then, horseradish peroxidase solution was placed on the top of the modified electrode for 4 hours. After 4 hours, the enzyme modified gold electrodes were washed with deionized water. Figure 3.21 shows mixture of nanomaterials with ethanol.

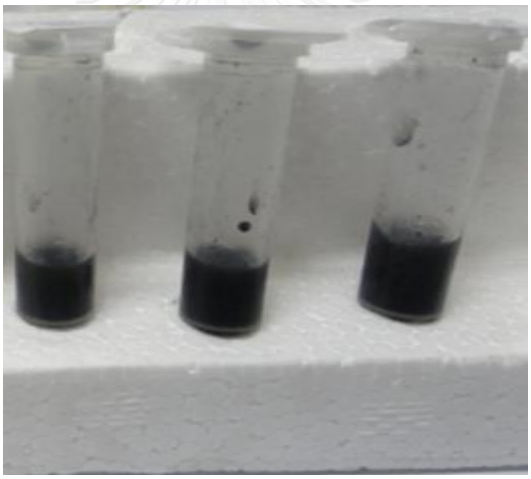

Figure 3. 21 Nickel oxide, manganese oxide and ethanol

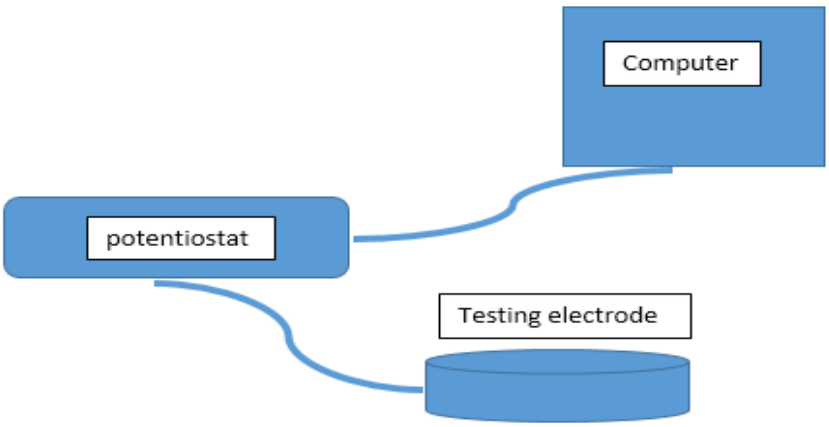

Figure 3. 22 Electrochemical sets- up

Figure 3.22 shows electrochemical experiment set up for cyclic voltammetry and amperometry testing. For cyclic voltammetry, the testing was conducted at potential from -1 V to 1 V and scan rates from 50 – 70 mV/s. The solution used for this testing is 1 mM potassium ferricyanide ($Fe(CN)_6$). For amperometry testing, the various concentration of hydrogen peroxide (3.18×10^{-5} M to 0.50×10^{-3} M) was used at potential at 0.3 V at the scan rate of 60 mV/s. Figure 3.23 shows electrochemical testing for commercial gold electrodes. 10 µl of each concentrations of hydrogen peroxide was placed on the top of gold electrodes.

Figure 3. 23 Electrochemical testing for commercial gold electrodes

Chapter 4
Results and Discussions

This chapter discusses about experiment result for carbon nanotube, transition metal oxide and sensors. The results will be separated in 3 sections. The first and second sections will present characterization of synthesized carbon nanotube and transition metals oxide. Transmission electron microscopy (TEM), Fourier transforms infrared spectroscopy (FTIR), Raman spectroscopy, Brunauer–Emmett–Teller (BET) and X-ray diffraction techniques were used to characterize these nanoparticle. The last section will discuss about characterization of fabricated sensors using electrochemical techniques.

4.1 Carbon nanotubes

4.1.1 Transmission Electron Microscopy (TEM)

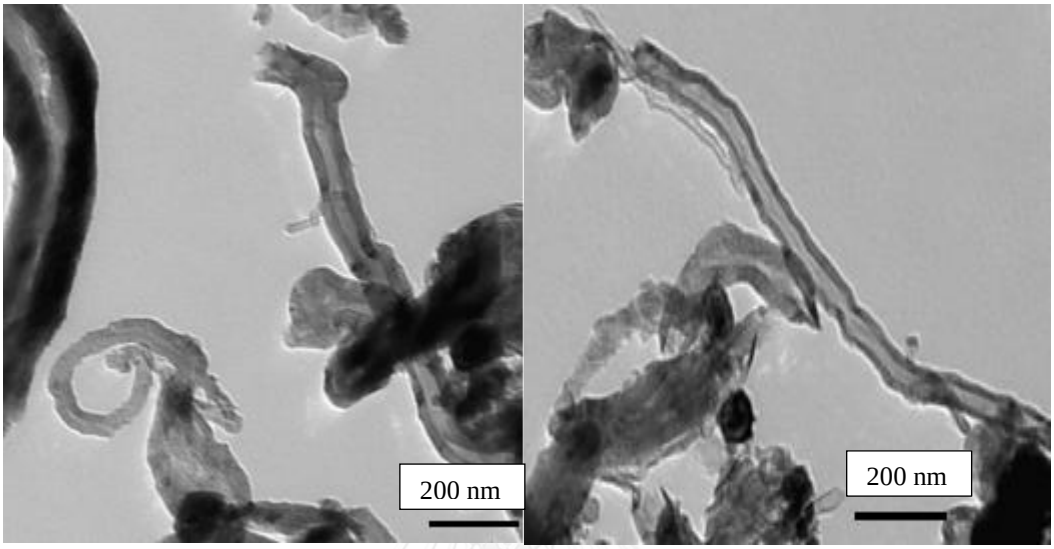

Figure 4. 1 TEM images for multi-walled carbon nanotubes

Figure 4.1 shown TEM image of multi-walled carbon nanotube. From the images, we can see that the number of wall of carbon nanotube is varied. The images also show amorphous carbon nanotubes also produced by using chemical vapor deposition technique. The estimated diameter for multiwall carbon nanotube 1, 2 and 3 are 50 nm, 80 nm and 210 nm, respectively.

4.1.2 Fourier Transform Infrared spectroscopy (FTIR)

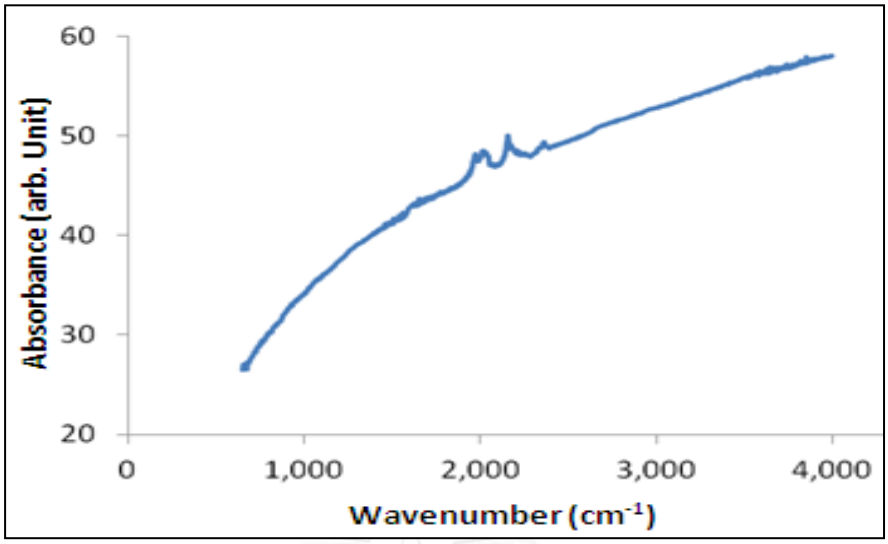

Figure 4. 2 FTIR spectrum of multi-walled carbon nanotube

Figure 4.2 shown FTIR spectrums for carbon nanotube before and after treatment. There is one small peak at 2000 cm^{-1} for multi-walled carbon nanotube before treatment, the peak become more obvious after treatments with sulfuric acid. Peak at 2000 cm^{-1} represent C≡C bonding.

4.1.3 Raman spectroscopy

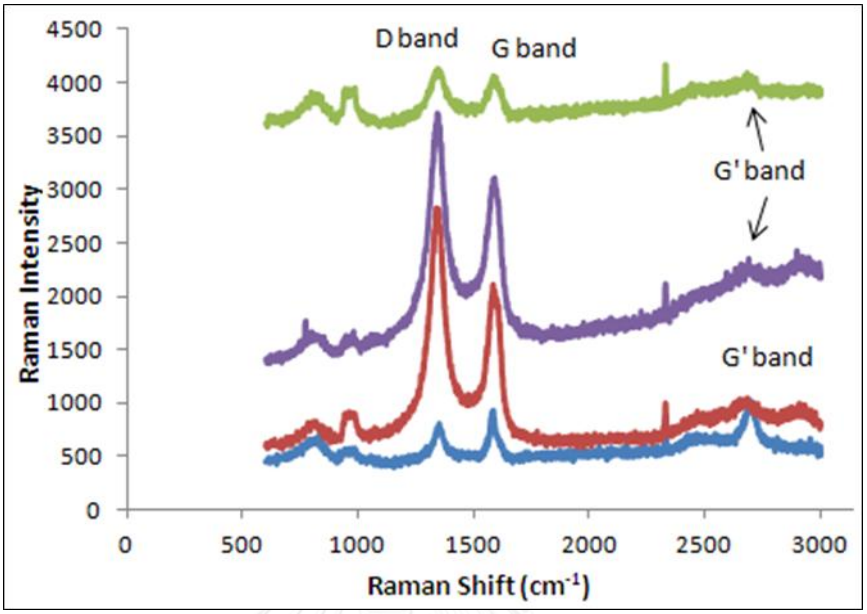

Figure 4. 3 Raman spectra for multi-walled carbon nanotube after treatment

Raman spectroscopy, a useful tool for the characterization of carbon materials, can provide structural information about the defects and tube alignment of MWCNTs [126]. Fig. 4.3 shown TEM image of multi-walled carbon nanotube at different points. The Raman band appearing in the 1500–1605 cm^{-1} region represent graphite band (G band) and the Raman band appearing in the 1250–1450 cm^{-1} region represent disorder band (D band) [127] .The D band is due to the A_{1g} breathing vibrations of sp^3 carbon atoms of defects and disorder while G band corresponds to E_{2g} mode vibra [128] . The intensity ratio of the D and G bands (ID/IG) is a good indicator to evaluate the integrity of carbon nanotubes [128].With ID/IG ratio increasing, the quality of carbon nanotubes decreased. In addition, the intensity ratio (ID/IG) for highest peaks of multi-walled carbon nanotubes is 1.44.

4.2. Metal oxides

4.2.1 Transmission Electron Microscopy (TEM)

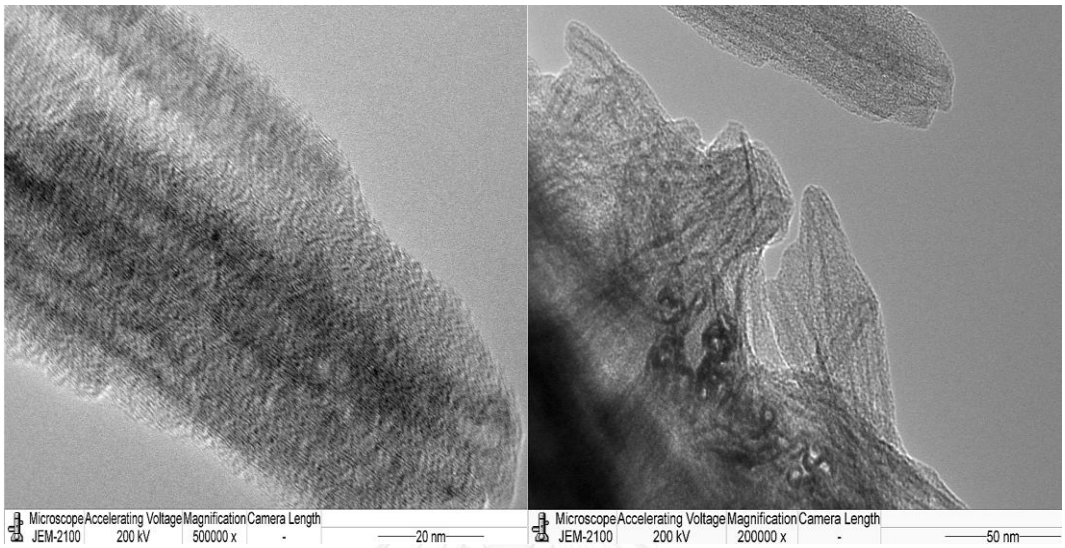

Figure 4. 4 TEM images of nickel oxide nanowires

The size and morphology was determined by TEM images. Figure 4.4 shows TEM images for 0.3 M nickel oxide. The image reveals that nickel oxide was in nanowires shape. The nickel oxide nanowires were in agglomerates form. Estimated mean diameter ranges from 2.4 - 4.8 nm and mean length ranges from 23.8 - 152.4 nm. The surface area for 0.3 M Nickel Oxide was 92.3 m^2/g. Thi Thanh Le Dang and Matteo Tonezzer synthesized polycrystal NiO nanowires using hydrothermal technique with a diameter about 20 - 50 nm which was bigger than our work because they used higher temperature which is 500 ^oC to annealing the nickel oxide compared to our work, 400^oC [129]. Adeela et. al fabricated nickel nanowires by electrodeposition in anodic aluminum oxide (AAO) with 98 nm of diameter and 17 μm of length which was also bigger size than our work [130].

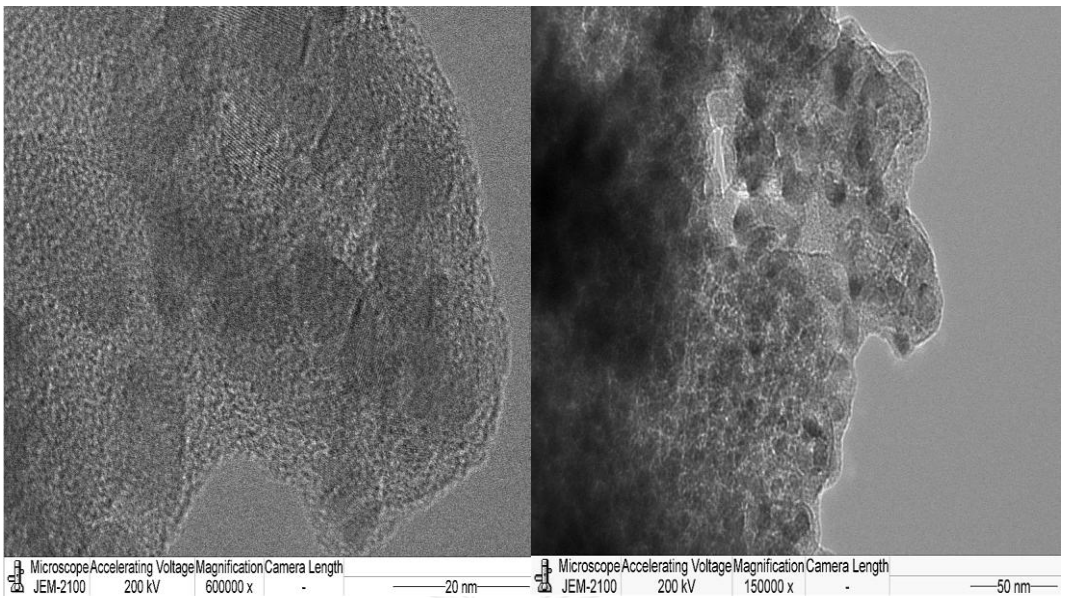

Figure 4. 5 TEM images of manganese oxide nanoparticles

Figure 4.5 shows TEM images for manganese oxide. The image reveals that manganese oxide was in nano speherical shape. The manganese oxide was in agglomerates form. Estimated mean diameter sizes ranges from 7.1 – 26.2 nm. The surface area for 0.5 M manganese oxide was 102.9 m^2/g. Azhar Z. Abbasi et. al synthesized hydrophobic MnO NPs at high temperature (~315 °C) with 5.3 nm and 13 nm in diameter [131]. Masoud S.N. et al. synthesized Mn_3O_4 nanoparticles using thermal decomposition with an average diameter of about 25 nm with the surface area about 130 m^2 /g [132]. He used Mn(sal) 2 -oleyl amine complex as a precursor and heated up to 100 ºC for 90 min. The resulting metal-complex solution was injected into 5 g of triphenylphosphine at 210 ºC. The black solution was aged at 210 ºC for 45 min, and was then cooled to room temperature.

4.2.2 Brunauer–Emmett–Teller (BET)

4.2.2.1 Nickel oxide

A) Effect the solvents

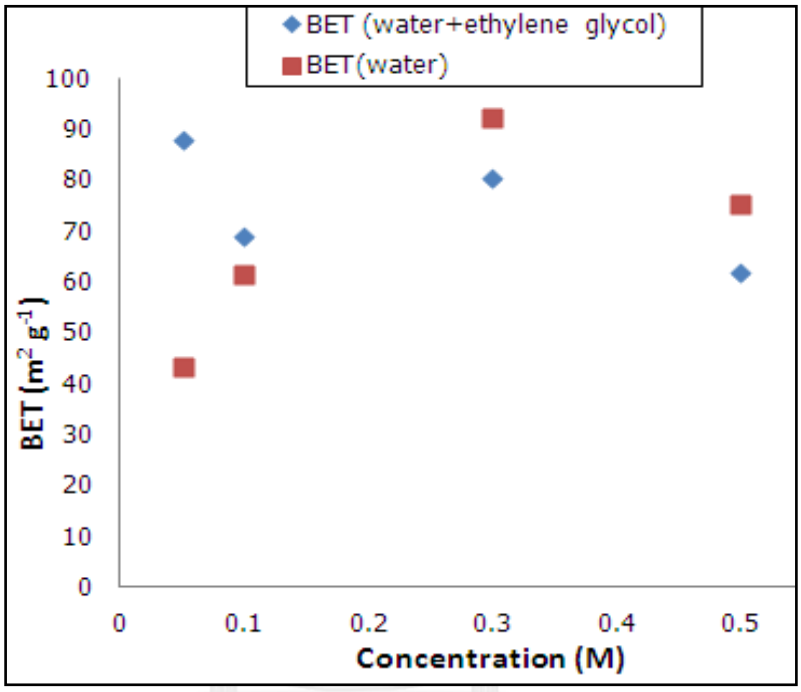

Figure 4. 6 Effect of solvents (deionized water and ethylene glycol) on nickel oxide surface area at 200°C for 7 hours

Figure 4.6 shows BET results for varying the concentration of nickel oxides nanoparticles prepared by different type of solvent. The red points are the data for water solvent and the blue points are the data for solvent which was the mixture of water and ethylene glycol. From the observation, different solvent resulted in the different value of surface area. The highest surface area was 92.3 m^2/g at 0.3 M NiO when the water was used as a solvent. It is known that the average particle size increases with viscosity of solvents. For our work, we used deionized water and ethylene glycol as a solvent during synthesizing nickel oxide. The viscosity of

deionized water is 1.01 x 10^{-3} Ns / m^2 and ethylene glycol is 1.61 × 10^{-2} Ns / m^2. Nasrin Talebian and Maryam Kheiri found that when they used different type of solvents which have different values of viscosity, they also found that the particle sizes of the NiO increased as the viscosity of solvent increased with the solvent viscosity [133].

B) Effect of temperatures

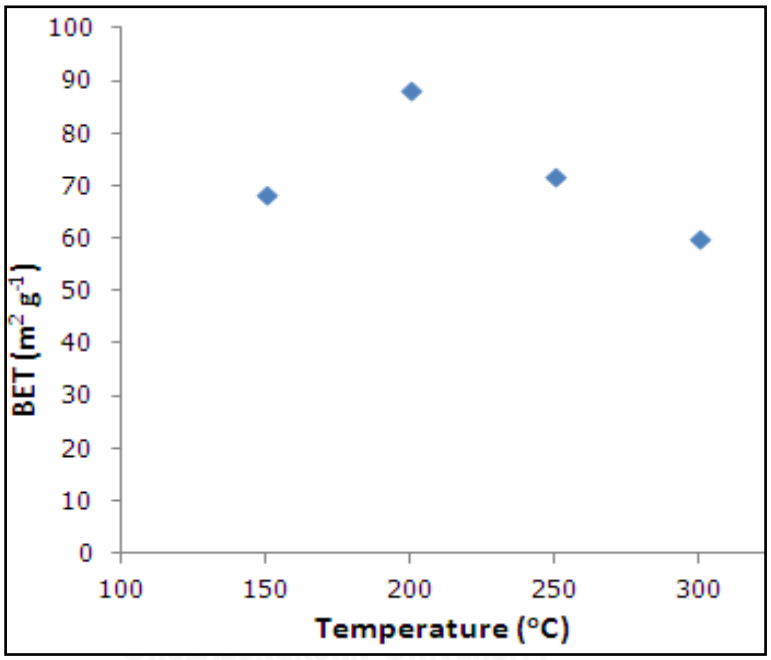

Figure 4. 7 Effect heating temperature on nickel oxide surface area at 0.05M for 7 hours

Figure 4.7 shows study on effect of temperature on surface area of the NiO nanoparticle. The highest surface area was obtained at 200 ^{o}C. In this situation, we used mixture of ethylene glycol and water as a solvent. The melting point of ethylene glycol is about 197.3°C, so at 300 ^{o}C all the etyhlene glycol will be completly evaporated Then when we increased the temperature, the grain growth phenomena took place and resulting in decreasing of the surface area of the nickel oxide

nanoparticles. In crystal formation by evaporation technique, the temperature affect is very important. The higher the temperature , the warmer the crystal solution will be, the faster the molecule will move. This movement allows them to evaporate more quickly, leaving particles behind to form into NiO crystals. If we increase the temperature more than 200^{o}C, the crystal start to grow. As a result the surface area decreased.

C) Effect of heating time

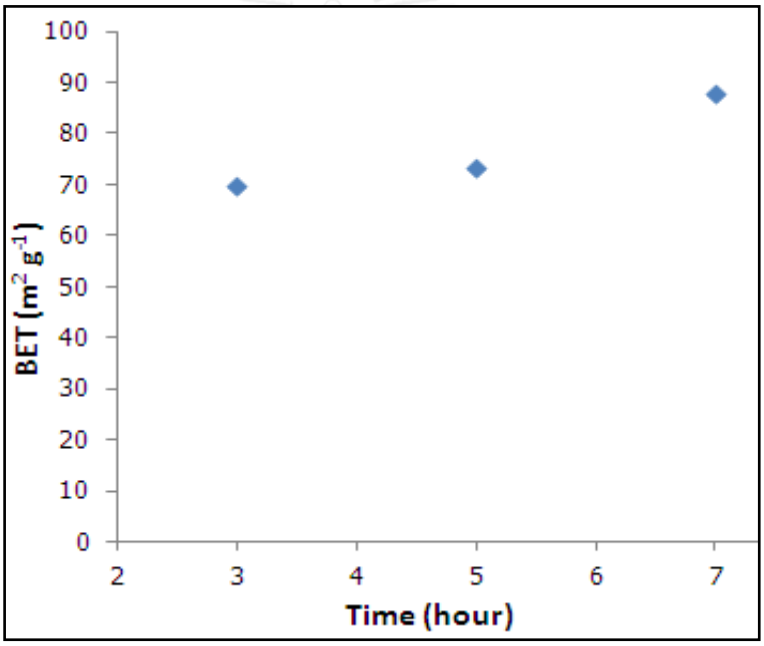

Figure 4. 8 Effect of heating time on nickel oxide surface area at 200 ^{o}C for 0.05 M

Figure 4.8 shows effect of the heating time on nickel oxide surface area. At 7 hours heating time gave highest surface area compared with 5 and 3 hours. This is because the increase of the heating time, in the presence of nucleuses and suitable operating conditions, results in a better growth process [134].

4.2.2.2 Manganese oxide

A) Effect of concentrations

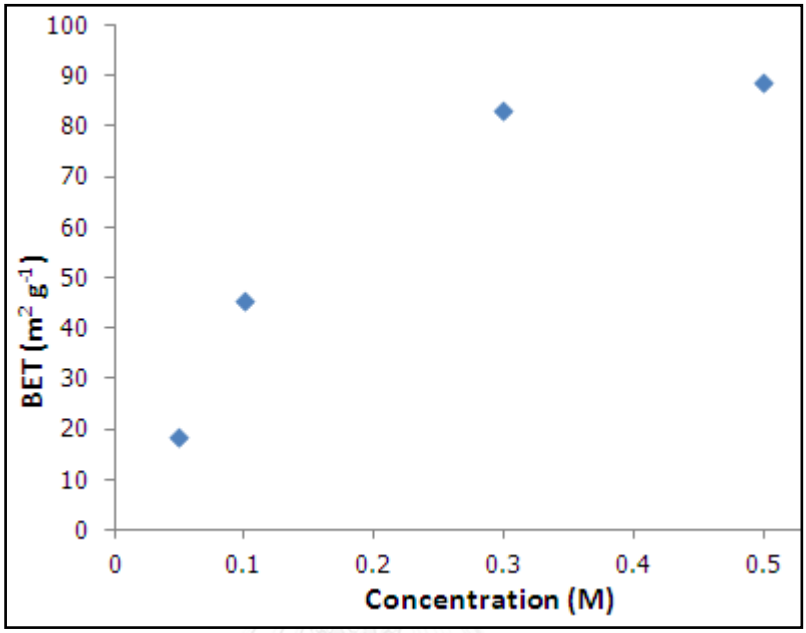

Figure 4. 9 Effect concentration on manganese oxide surface area at 125 ^{o}C for 3 hours

Figure 4.9 shows effect of concentrations for manganese oxide surface area. The solvent used was dionized water. It is well known that increasing or decreasing the concentration of the chemical reactants will eventually influence the resultant products. As the concentrations of manganese acetate increased, the surface area also increased. When higher of concentration of saturated solution was used, the crystal in smaller sizes will produced [135]. The smaller the crystals size, the higher the concentration of the of the saturated solution. Solubility corresponds to saturation. Solubility, Cr is related to the mean radius r of the crystal by the relationship, valid for $r \neq 0$ [135] :

$$C_r = C_e \exp(2v_m\gamma_i/kTr) \quad (24)$$

where v_m is the molecular volume, γ the interfacial specific energy, k the Boltzman constant.

B) Effect of temperatures

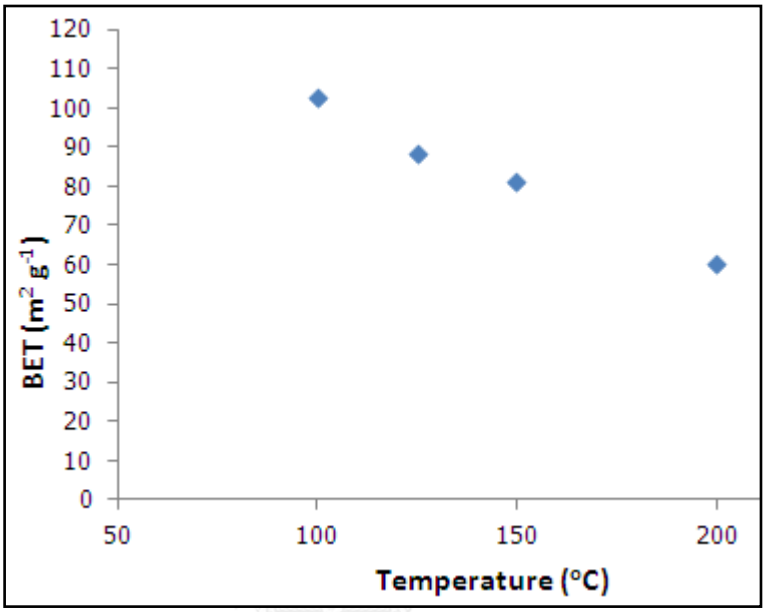

Figure 4. 10 Effect temperature on manganese oxide surface area for 0.5 M at 3 hours

Figure 4.10 shows effect of heating temperature on manganese oxide. When heating temperature increased, the surface area of manganese oxide decreased. It might be because of the solvent that we used during preparation. Water boiling temperature is 100 ^{o}C. So at 100 ^{o}C, the water completely dries and lefts the manganese particles. As a heating tenmperature increases, the particles start to growth and resulted in decreasing in surface area.

4.3 X-Ray Diffraction (XRD)

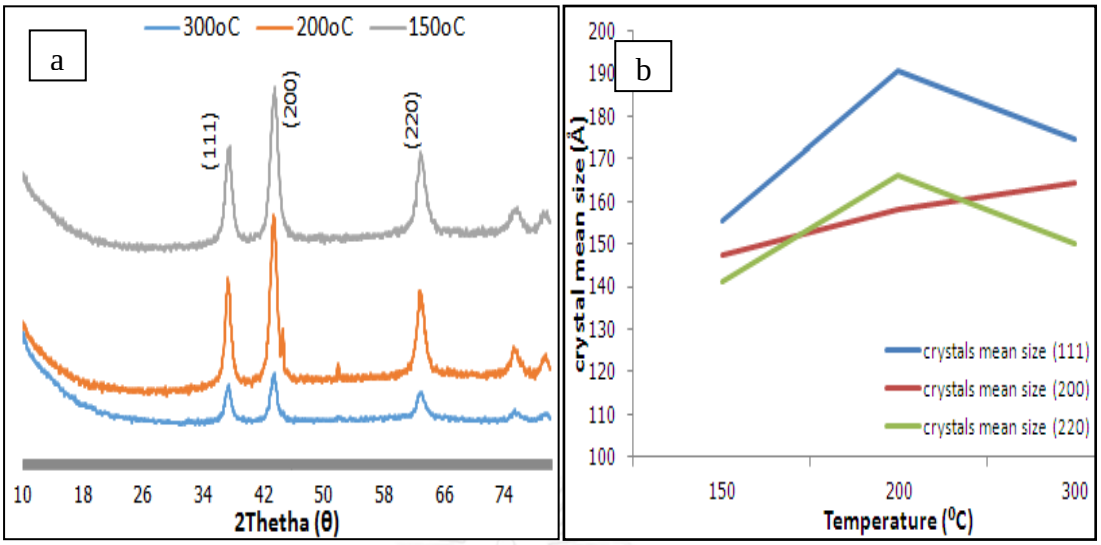

Figure 4. 11 Nickel oxide 0.05 M (EG:DI) at 300 ^{o}C, 200 ^{o}C and 150 ^{o}C (a) XRD patterns; (b) crystal mean size

Figure 4.11 (a) shows XRD patterns for 0.05 M nickel oxide at different heating temperature. Three main peasks were observed. They represent (111) (200) and (220) planes [136]. From the XRD patterns, the highest crsystalline peak can be observed at 200 ^{o}C. The lowest crsytalline peak can be observed at 300 ^{o}C as shown in Figure 4.11 (a). The relation between the temperature and mean crystal sizes can be observed at Figure 4.11 (b). Crystal mean size for 0.05 M nickel oxide at different temperature range from 150 – 300 ^{o}C. The highest crystal mean size for plane (111) and (220) happen at 200 ^{o}C. For (200) plane, the highest crystal mean size at 300 ^{o}C. Different plane produced different crystal mean size might be due to effect of temperature When heat was applied, the atom in a crystal will vibrate lead to an angle dependent effect on the diffracted peak intensities.

The more an atom vibrates the scattering power is decreased. It is because the scattering power can caused atom to smeared out. Temperature factor can be expressed [137]:

$$TF(\theta) = exp(B(sin\theta/\lambda)^2) \quad (25)$$

where the coefficient B is the isotropic temperature factor.

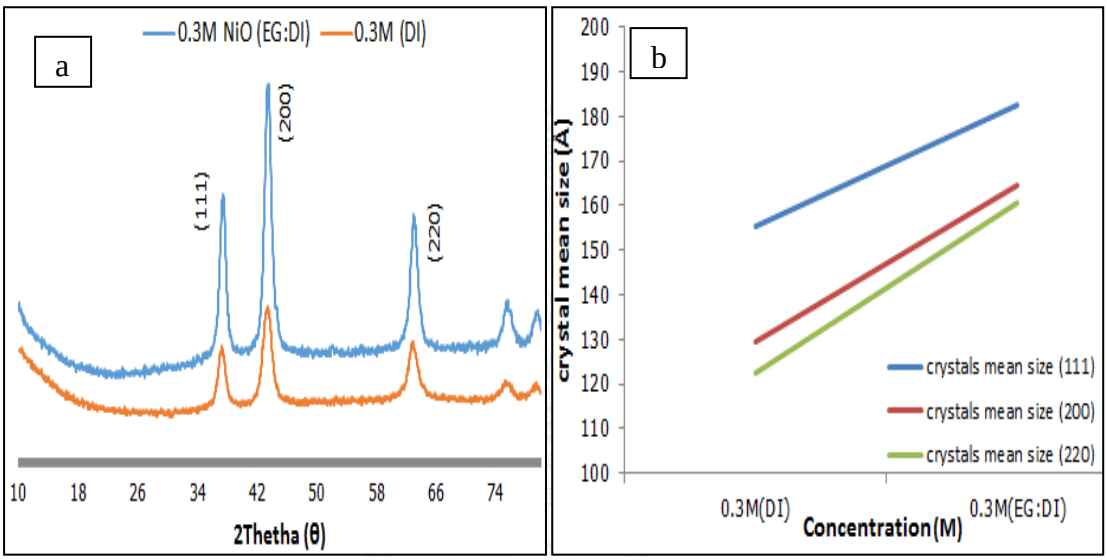

Figure 4. 12 Nickel oxide 0.3 M at 200°C for 7 hours, (a) XRD patterns; (b) crystals mean size

Figure 4.12 (a) shows the XRD patterns for 0.3M nickel oxide at 200 °C at 7 hours. There is no diffetent in crystal plane obtained from different solvent. However at the same concentration, the higher crystalline peak was observed when the mixture of ethylene glycol comparing to the used of deionized water as solvent. The solvent mixture of deionized water with ethylene glycol has higher viscosity compare solvent only with deionized water. It is because in solution growth, these growth units are typically solvated, closely surrounded by a number of solute molecules that must be

rejected at the growing crystal interface. The solvent may influence crystal growth through its effect on viscosity, molecular density, diffusivity, heat and mass transport [138]. Since diffusion is inversely proportional to solvent viscosity, it will cause rapid diffusion in hydrithermal growth. The nickel was easily dissolved in water.

The smaller the crsytsal size, the higher the concentration of the of the saturated solution. The relation between solubility and saturation can be expressed followed Equation 24.

where v_m is the molecular volume, γi the interfacial specific energy, T is temperature and k the Boltzman constant.

Figure 4.12 (b) shows crystals mean size for 0.3 M nickel oxide at 200 ^{o}C for 7 hours. The lower crystals mean size were obtained when water was used to synthesize the nickel oxide at 200 ^{o}C. This implies that the higher surface area of the nickel oxide was obtained when the water was used as solvent. This result confirms the BET results in Figure 4.6 that water solvent gave the higher surface area.

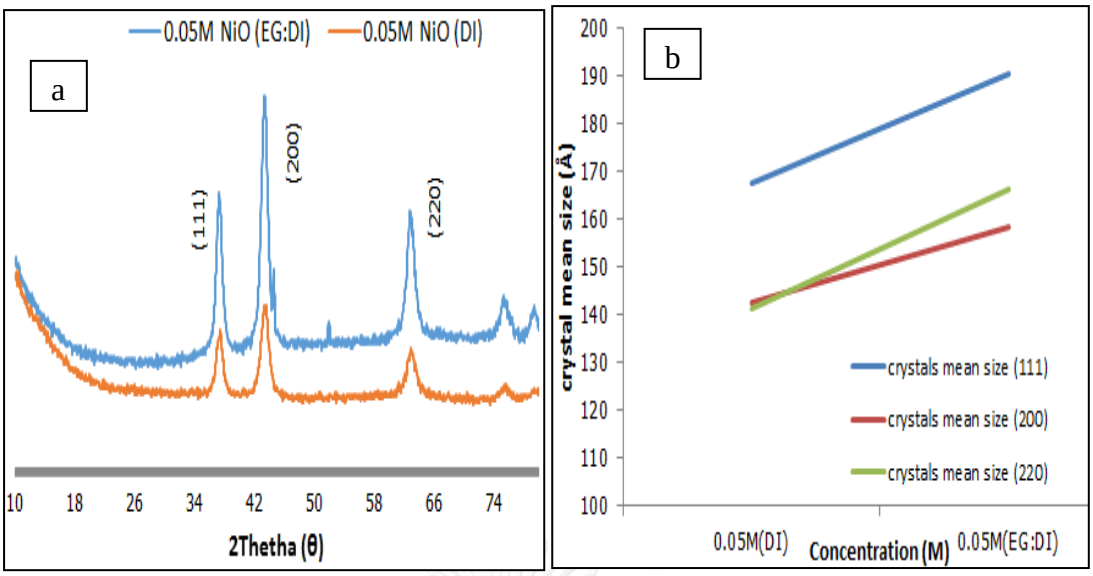

Figure 4. 13 Nickel oxide 0.05 M at 200^{o}C for 7 hours; (a) XRD patterns; (b) crsytals mean size

Figure 4.13 (a) shows XRD patterns for 0.05 M nickel oxide at 200 ^{o}C for 7 hours. The same phenomena was observed for 0.05 M nickel oxide. The highest crystalline peaks were observed when the mixture solvent of deionized water and ethylene glycol is used to synthesize nickel oxide. Figure 4.13 (b) shows crsytals mean size for 0.05 M nickel oxide at 200 ^{o}C for 7 hours. The lower crsyatls mean size was obtained when water solvent was used to synthesize the nickel oxide at 200 ^{o}C . This implies that the higher surface area of the nickel oxide was obtained when the water was used as solvent. This result confirms the BET results in Figure 4.6 that water solvent gave the higher surface area.

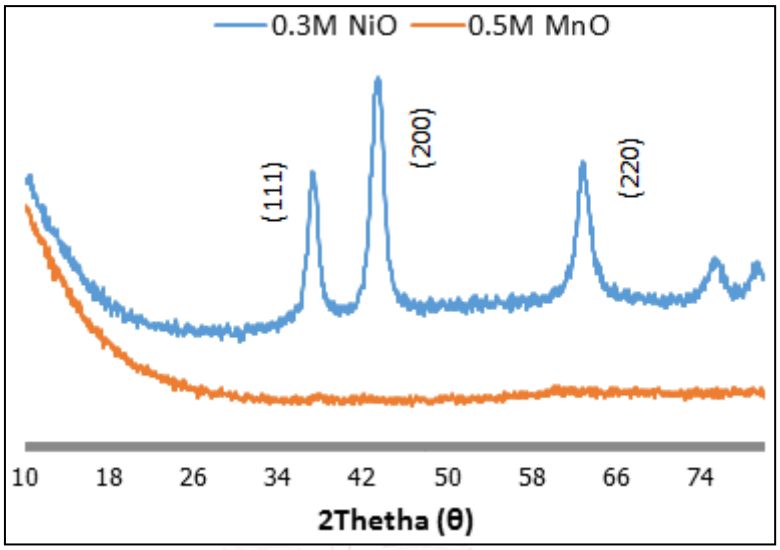

Figure 4. 14 XRD patterns for 0.3 M nickel oxide (deionized water) at 200°C for 7 hours and 0.5 M manganese oxide at 100°C for 3 hours.

Figure 4.14 shows XRD results for the nickel oxide comparing with the manganese oxide. From the graph, it should be noted that the high crystalline was observed from the nickel oxide while the amorphous structure was observed from the manganese oxide. These 2 metal oxide were mixed togerther using ethanol to form a binary catalysts for sensor fabrication

4.4 Sensors

4.4.1 Cyclic voltammetry

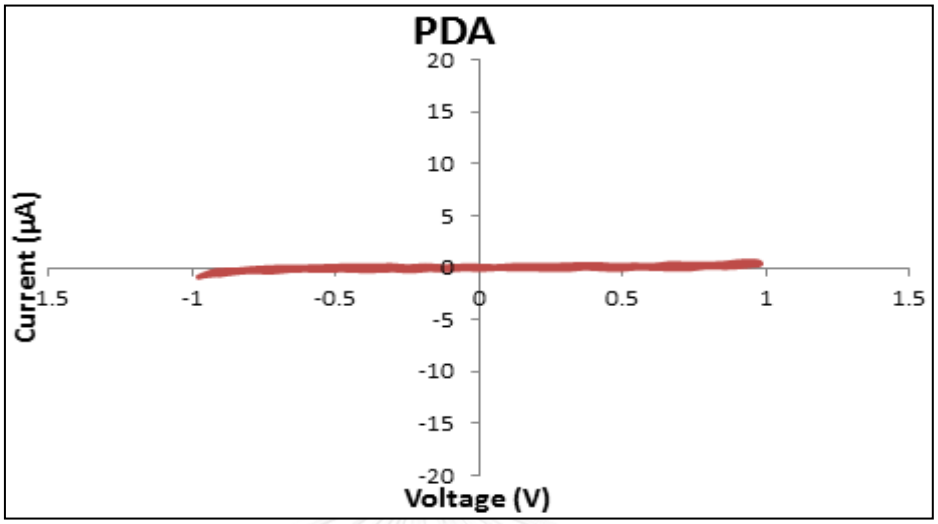

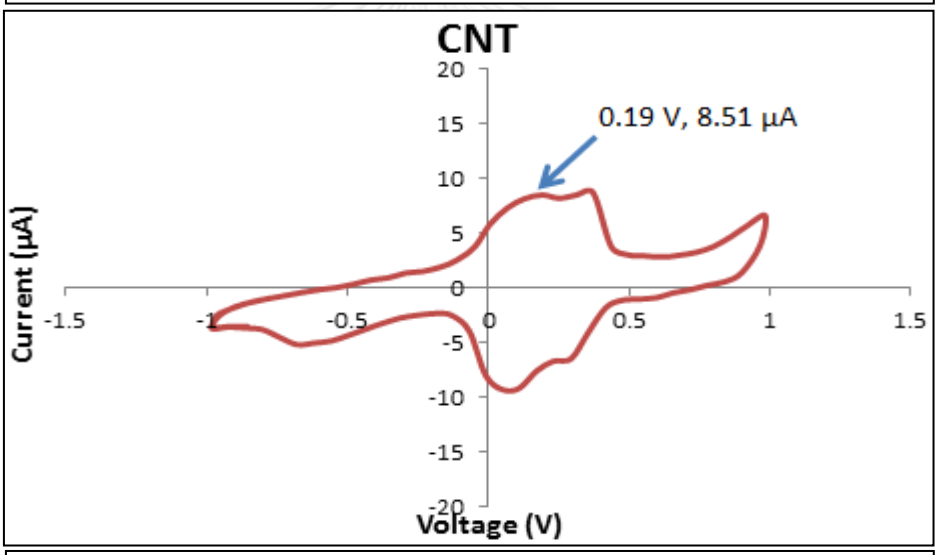

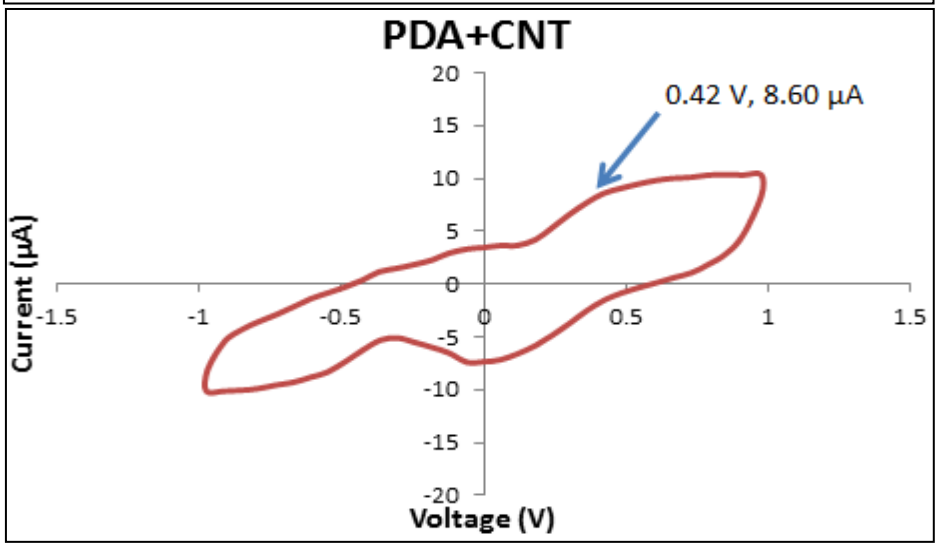

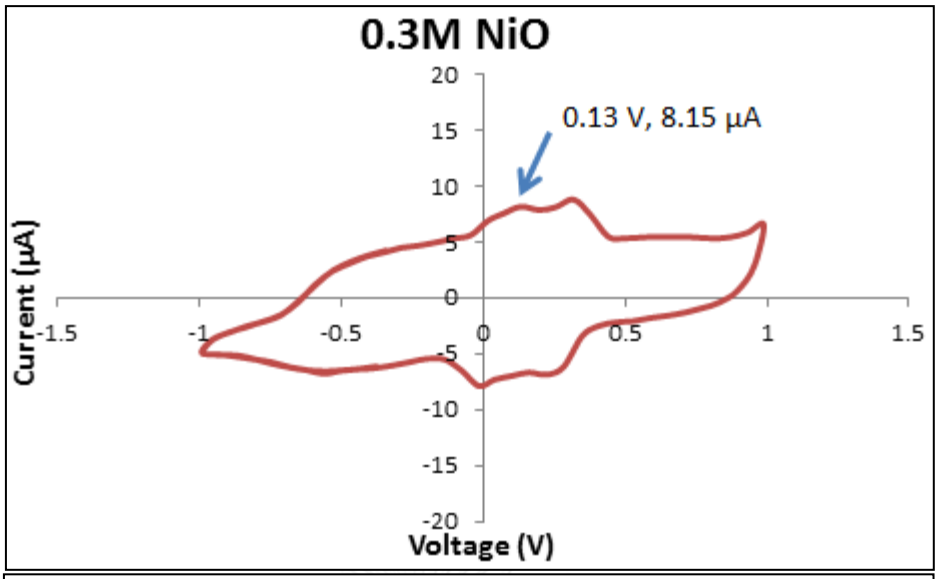
0.3M NiO
0.13 V, 8.15 µA
Current (µA)
Voltage (V)
20
15
10
5
0
-5
-10
-15
-20
-1.5
-1
-0.5
0
0.5
1
1.5

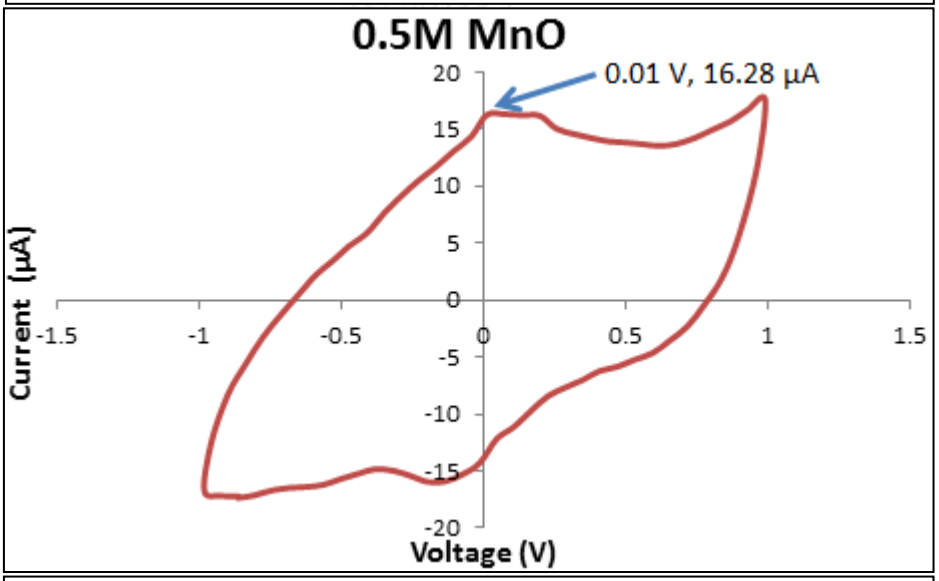
0.5M MnO
0.01 V, 16.28 µA
Current (µA)
Voltage (V)
20
15
10
5
0
-5
-10
-15
-20
-1.5
-1
-0.5
0
0.5
1
1.5

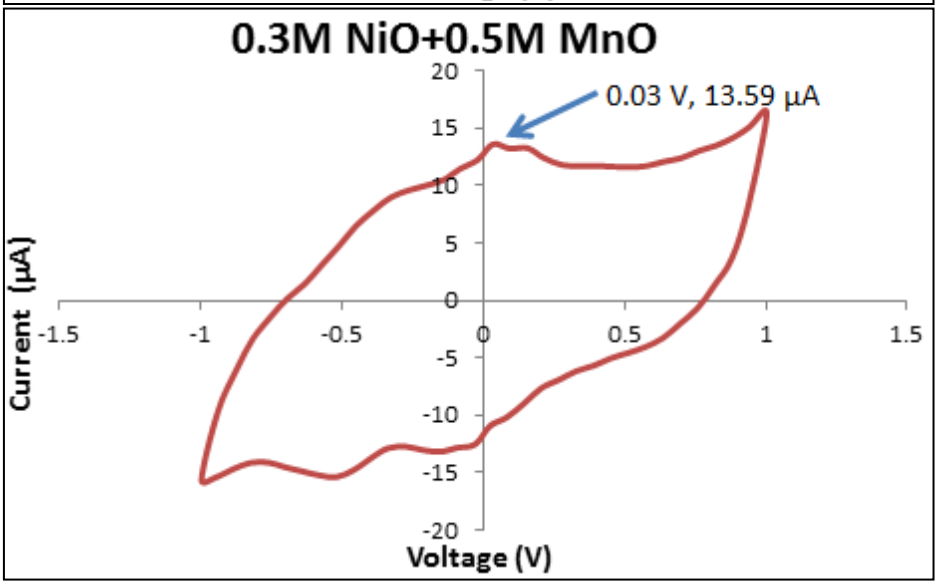
0.3M NiO+0.5M MnO
0.03 V, 13.59 µA
Current (µA)
Voltage (V)
20
15
10
5
0
-5
-10
-15
-20
-1.5
-1
-0.5
0
0.5
1
1.5

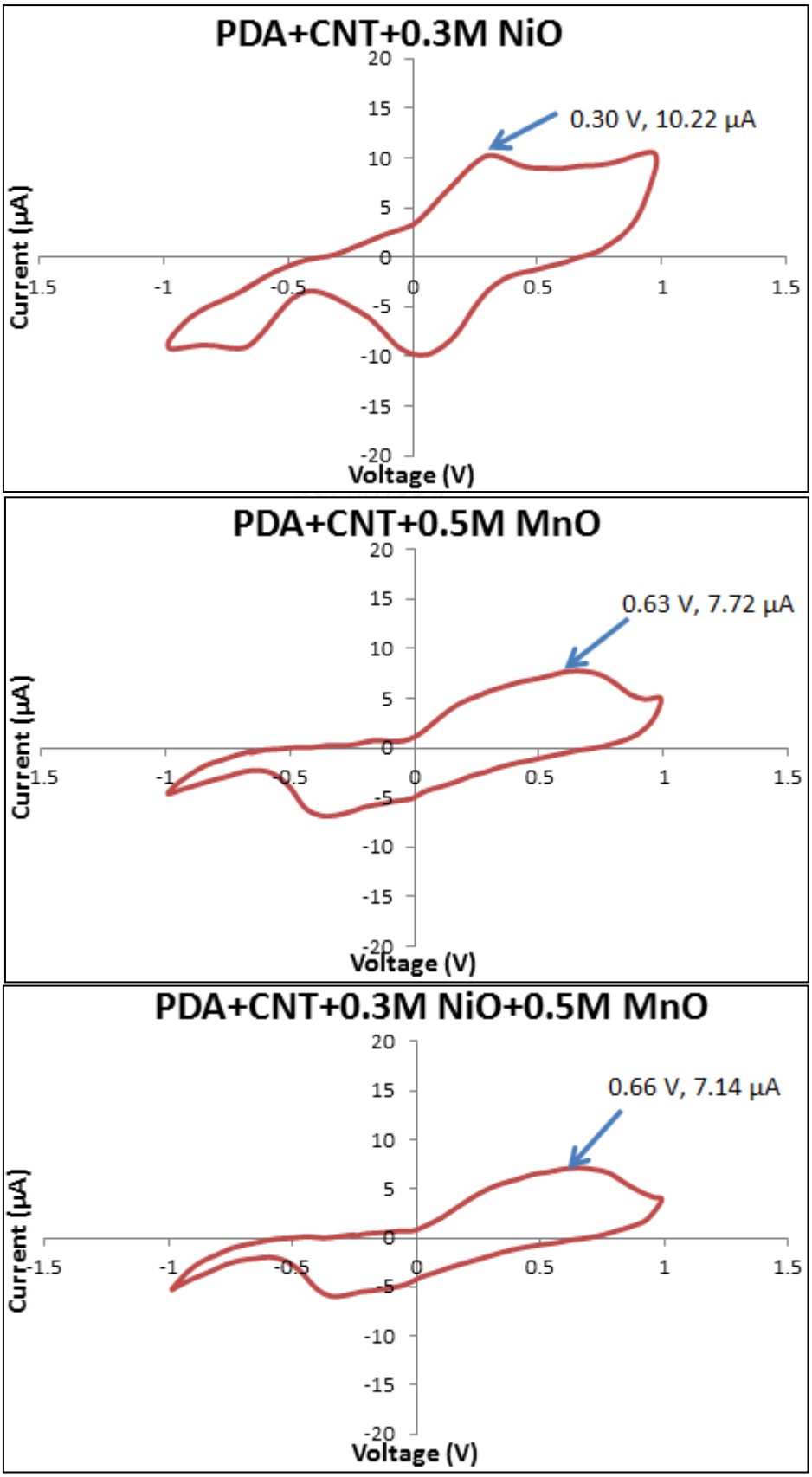
PDA+CNT+0.3M NiO
0.30 V, 10.22 µA
Current (µA)
Voltage (V)
PDA+CNT+0.5M MnO
0.63 V, 7.72 µA
Current (µA)
Voltage (V)
PDA+CNT+0.3M NiO+0.5M MnO
0.66 V, 7.14 µA
Current (µA)
Voltage (V)

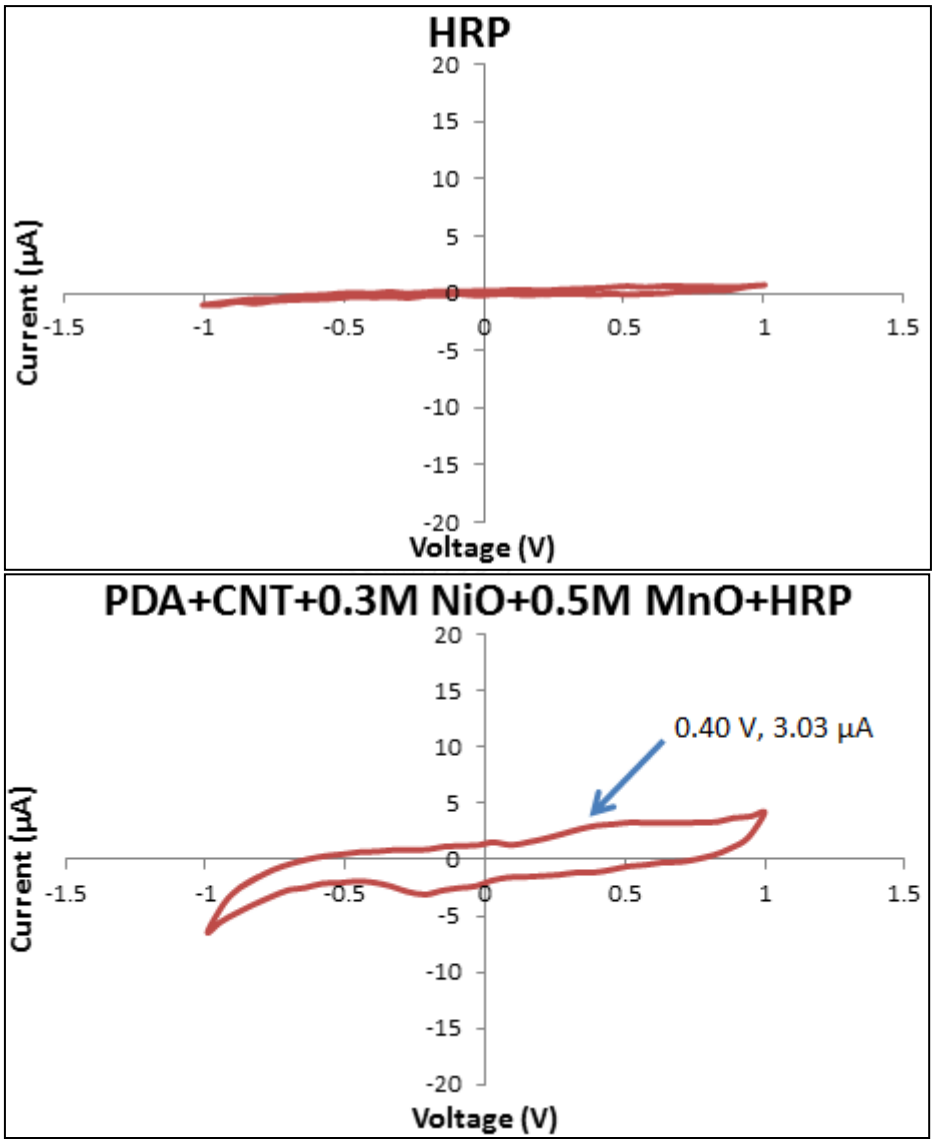

Figure 4. 15 Cyclic voltammetry of modified gold electrodes from -1 V to +1 V at scan rate 60 mVs^{-1} using 1mM of ferricyanide. All curves correspond to 3rd cycle.

Figure 4.15 show cyclic voltammetry for all modified gold electrodes. The cyclic voltammetry graph provides information about oxidation potential for every modified gold electrode. Table 4.1 is summary for redox potential and current all modified gold electrode. Potassium ferricyanide (1 mM) a strong redox chemical was used to study about oxidation and reduction of the modified electrodes. Modified gold electrode with 0.5M MnO has lowest oxidation potential which is 0.01 V. The highest oxidation

potential is modified gold electrode with binary catalyst 0.3M NiO+0.5M MnO which is 0.66 V. When gold electrode was immobilized with HRP enzyme, there is no redox peak can be observed due to denature of enzyme. Enzyme is very sensitive to the temperature and pH, so pottasium ferricyanide might denature the enzyme. However the performance of modified gold electrodes with enzyme will be different in amperometry testing. With present of HRP enzyme, the current produced will be increased. Polydopamine is a natural polymer and it was used as a coating material for this work. There is no redox can be observed at voltammetric graph for polydpamine. It is because polydopamine is an insulator material and no electron transfer on the electrode surface after coating with polydopamine. The highest oxidation currents were produced at gold electrode modified with 0.5M MnO, 0.3M NiO+0.5M MnO and PDA+CNT+0.3M NiO. It indicates that manganese oxide have higher catalyst activity more than nickel oxide. It might be because the concentration and surface area of manganese oxide is higher than nickel oxide.

Table 4. 1 Redox potential and current for modified gold electrodes

No	Modified Gold Electrode	I_{ox} (µA)	E_{ox} (V)	I_{rd} (µA)	E_{rd} (V)
1	Bare Au	3.12	0.13	-2.80	-0.26
2	HRP	-	-	-	-
3	PDA	-	-	-	-
4	CNT	8.51	0.19	-9.30	0.05
5	0.3M NiO	8.15	0.13	-6.86	0.23
6	0.5 M MnO	16.28	0.01	-15.91	-0.14
7	0.3M NiO + 0.5M MnO	13.59	0.03	-13.17	-0.15
8	PDA+CNT	8.60	0.42	-7.40	-0.06
9	PDA+CNT + 0.3M NiO	10.22	0.30	-9.74	-0.005
10	PDA+CNT +0.5M MnO	7.72	0.63	-6.81	-0.39
11	PDA+CNT +0.3M NiO+0.5M MnO	7.14	0.66	-5.93	-0.34
12	PDA+CNT +0.3M NiO+0.5M MnO+HRP	3.03	0.40	-3.09	-0.22

4.4.2 Amperometry.

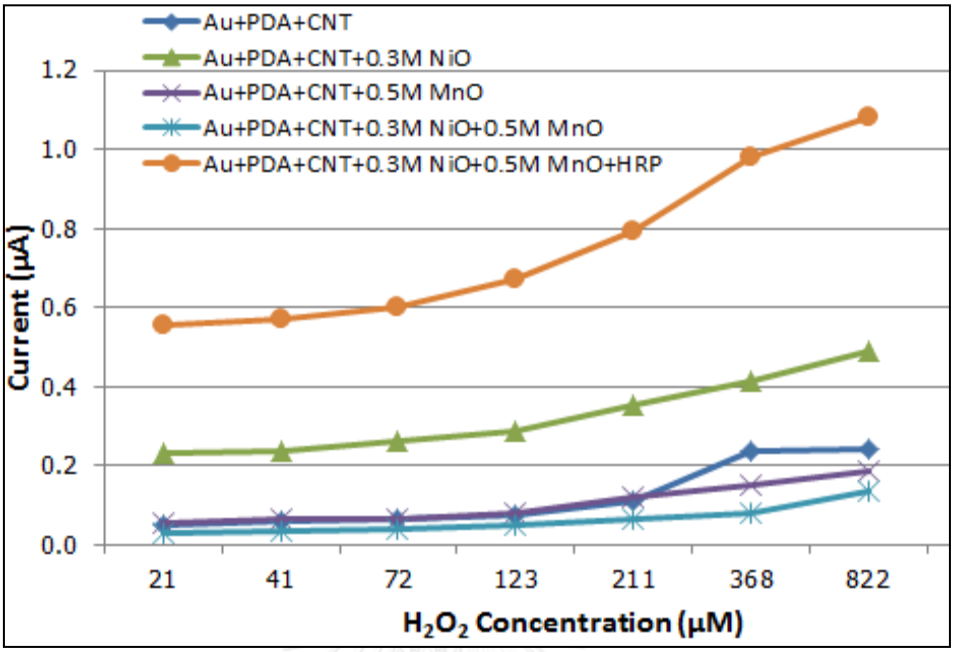

Figure 4. 16 Amperometric responses for modified gold electrodes with different concentration of H_2O_2 at applied potential of 0.3 V

Figure 4.16 shows calibration curve for 5 modified gold electrodes. The lowest amperometric respond is modified gold electrode with binary catalyst. Modified enzyme gold electrode with binary catalyst is the highest amperometric respond. Different concentrations of hydrogen peroxide from 21 – 822 µM were used. The potential was used for this testing 0.3 V and it a lowest oxidation potential that can be obtained at modified electrode with PDA, CNT and 0.3M NiO. The lowest potential was selected to avoid any interference such as nitric acid. As mentioned in cyclic voltammetry section, the performance of enzyme modified electrode will be higher in this testing. As a result, modified gold electrode with binary catalyst and enzyme has highest amperometric respond compare to others modified gold electrodes. This is due to catalyst activity of horseradish peroxidase enzyme on hydrogen peroxide. Modified

gold electrode with PDA, CNT and 0.3M NiO also give higher amperometric respond due to lowest oxidation potential that can be obtained at Table 4.1.

Chapter 5
Conclusion and Recommendation

This chapter will conclude all the experimental results that already discussed in Chapter 4. Some recommendations also will be presented in transition metal oxides synthesize process and applications for further improvement.

5.1 Conclusions

From our works we can conclude that:

1) Nanomaterials nickel oxides and manganese oxides were successfully synthesized by using hydrothermal technique.
2) To study the optimum surface area of nickel oxides and manganese oxides, experiment parameters such as heating temperature, heating time and concentration were varied.
3) TEM images revealed morphology of nickel oxides was in nanowires with estimated diameter about 2.4 - 4.8 nm. For manganese oxides, the morphology was nanoparticle in spherical form with the estimated diameter 7.14 – 26.2 nm.
4) Crystallization studies revealed effect of heating temperature, concentration and solvent to the crystals size. The smallest crystal size that can be obtained in this work is 13 nm at 0.3 M of nickel acetate with heating temperature 200 ^{o}C for 7 hours.

5) Layer by layer modified gold electrodes were fabricated by using a simple techniques which was dropped and dried at room temperature.
6) Cyclic voltammetry exhibits electrochemical responses corresponding to the modified gold electrode surfaces. Both bare gold electrode and polydopamine modified gold electrode exhibit almost no voltammetric response. After deposited single or binary catalysts on the electrode surfaces, the voltammetric responses were greatly improved. The highest voltammetric response was obtained at modified gold electrode with 0.5 M manganese oxide which is 16.28 μA at 0.01 V.
7) The modified gold electrode with binary catalyst and enzyme showed highest amperometric response which is 1.1 μA at 822 μM concentration of hydrogen peroxide. The excellent sensing activity by modified gold electrode with binary catalyst and enzyme might be attributed from catalyst activity from horseradish peroxidase.

Table 5.1 and 5.2 shows the comparison between our work and the other researchers work for nickel oxides and manganese oxides. For both metal oxides synthesized by our work, we can obtain higher surface area by using low heating temperatures and shorter heating times. For example, Guangmei Bai et. al. used 24 hours to obtained nickel hydroxide at room temperature. In comparison with our work, we only need 7 hours to obtained nickel hydroxide at 200 °C [139]. Guangmei Bai et. al. also obtained lower surface area of nickel oxides is about 5.6 m^2/g compare with our works 92 m^2/g [139]. Baoping Lu et. al. obtained the highest surface area for nickel hydroxide [141]. However he required longer heating time compared with our work

which is 48 hours. In our work, we used 100 °C for 3 hours to synthesized manganese oxide. Li Zhou et al. used longer heating times 12 hours to synthesized manganese oxide but has lowest surface area compared with our work [142].

Table 5. 1 Comparisons of process parameters for nickel oxides

Catalyst	Synthesis Technique	Size	Temperature/Time	Application	Reference
$Ni(OH)_2$	hydrothermal	-	200 °C for 7 hours	H_2O_2 biosensor	Our work
NiO	calcined	2.4-4.8 nm (D), 23.8-152.4 nm (L), 92 m^2/g	400 °C for 2 hours		
$Ni(OH)_2$	microemulsion	-	room temperature for 24 hours	toluene combustion	Guangmei Bai et. al [139]
NiO	calcined	5.6 m^2/g	400 °C, 3 hours		
$NiC_2O_4 \cdot 2H_2O$	hydrothermal	2-4 µm (L) and 80-100 nm (D)	180 °C for 20 hours	gas sensor	Zeng Wen et. al. [140]
NiO	calcined	2-3 m (L) and 85-100nm (D)	400 °C, 2 hours		
$(Ni(OH)_2$ OMCs)	hydrothermal	275 m^2/g	180 °C for 48 hours.	ethanol sensor	Baoping Lu et. al.[141]

Table 5. 2 Comparisons of process parameters for manganese oxides

Catalyst	Synthesis Technique	Size	Temperature/Time	Application	Reference
MnO	hydrothermal	103 m^2/g	100 °C for 3 hours.	H_2O_2 biosensor	Our work
MnO	hydrothermal	94.6 m^2/g	120 °C for 12 hours.	Formaldehyde oxidation	Li Zhou et. al. [142]

5.2 Future recommendations

Electrochemical hydrogen peroxide sensors were fabricated using commercial gold electrodes. The metal oxides catalyst was synthesized using hydrothermal technique. The surface area obtained from this process is between 8.2 m^2/g to 102.9 m^2/g. Because the sensitivity of the sensor is related to surface area, so if we can synthesize metal oxides larger surface area, it will increase the sensitivity. Besides hydrothermal technique, inert gas condensation is one of good technique to produce high purity of nanocrystals and more large surface area. In our work, metal oxides catalyst was used to detect hydrogen peroxide at room temperature. The highest current produced from the electrochemical reaction was about 1.1 μA at 822 μM of hydrogen peroxides. Besides hydrogen peroxide sensor, this catalyst also can be applied in high temperature application, for example in gas sensor. The catalyst activity at high temperature is higher than at room temperature, therefore the current produced also will increase.

REFERENCES

1]. S. Su, W.W., J. Gao, J. Lub, C. Fan, *Nanomaterials-based sensors for applications in enviromental monitoring.* Journal of Materials Chemistry, 2012. **22**(35): p. 18101-18110.

[2]. T.Seiyama, N.Y., K. Eguchi, *Characterization and activity of some mixed oxide catalysts.* Industrial & Engineering Chemistry Product Research and Development, 1985. **1**(24): p. 19-27.

[3]. A.M.El-Sharkawy, *Electrical conductivity measurements of mixed oxide catalysts used as a typical reaction of heavy water production*, in *International Journal of Chemistry and Material Science*. 2013. p. 55-68.

[4]. A.A.Ansari, M.A., M.S. Alsalhi, A.S. Aldwayyan, , *Nanostructured Metal Oxides Based Enzymatic Electrochemical Biosensors*. 2010, InTechOpen. p. Chapter 2.

[5]. Q. Kuang, X.W., Z. Jiang, Z. Xie, L. Zheng, *Highe Energy Surface Engineered Metal Oxide Micro and Nanocrystallites and Their Applications.* Accounts of Chemical Research, 2014. **2**(47): p. 308-318.

[6]. J. Wang, X.C.Z., *Core-Shell Magnetic Nanoclusters*. 2009, Spinger.

[7]. G.Singh, I.P.S.K., S. Dubey, *Bimetallic nanoalloys: Preparation, characterization and their catalytic activity.* Journal of Alloys and Compounds, 2009. **480**(2): p. 270-274.

[8]. F. Tao, M.E.G., Y. Zhang, D.R. Butcher, J.R. Renzas, Z. Liu, J.Y. Chung, B.S. Mun, M. Salmeron, G.A. Somorjai, *Reaction-driven restructuring of Rh-Pd and Pt-Pd core-shell nanoparticles.* Science, 2008. **322**: p. 932-934.

[9]. H. Idriss, M.S., J. Llorca, S.C. Chan. W. Chiu, P.Y. Sheng, A. Yee, M.A. Blackford, S.J. Pas, A.J. Hill, F.M. Alamgir, R. Rettew, C. Petersburg, S.D. Senanayake, M.A. Barteau, *A phenomenological study of the metal-oxide interface: The role of catalysis in hydrogen production from reneable resources.* Chemistry & Sustaibility Energy & Materials, 2008. **1**(11): p. 905-910.

[10]. N.J. Divins, E.L., A. Rodriguez, D. Vega, J. Llorca, *Bio-ethanol steam reforming and autothermal reforming in 3um channels coated with RhPd/CeO2 for hydrogen generation.* Chemical Engineering Process, 2013(64): p. 31-37.

[11]. G.A. Deluga, J.R.S., L.D. Schmidt, X.E. Verykios, *Renewable hydrogen from ethanol by autothermal reforming.* Science, 2004(303): p. 993-997.

[12]. J. Llorca, V.C.C., N. J. Divins, R.O. Fraile, E. Taboada, L. M. Gandia, G. Arzamendi, P.M. Dieguez, Renewable Hydrogen Technologies, 2013: p. 135-169.

[13]. M.S. Wong, O.J.J.A., Y.L. fang, N. Ak, M.O. Nutt, J,T, Millere, K. N. Heck, *Cleaner water using bimetallic nanoparticles catalyst.* Society of Chemical Industry, 2008(84): p. 158-166.

[14]. H. Lee, J.R., P.B. Messersmith, *Facile conjugation of biomolecules onto surfaces via mussel adhesive protein inspired coatings.* Advanced Materials, 2009(21): p. 431-434.

[15]. M. Li, C.D., Q. Xie, Y. Yang, S. Yao, *Electrochemical quartz crystal impedance study on immobilization of glucose oxidase in a polymer grown*

from dopamine oxidation at an Au electrode for glucose sensing. Electrochimica Acta, 2006(51): p. 5478-5486.

[16]. Ajayan, P.M., *Nanotubes from carbon.* Chemical Revision, 1999(99): p. 1787-1800.

[17]. Y.P. Sun, K.F.F., Y. Lin, W.J. Huang, *Functionalized carbon nanotubes: properties and applications.* Accounts of Chemical Research 2002(35): p. 1096-1104.

[18]. N. Halonen, A.R., A.R. Leino, T. Kyllonen, G. Toth, J. Lappalainen, K. Kordas. M. Huuhtanen, R.L. Keiski, A. Sapi, M. Szabo, A. Kukovecv, Z. Konya, I. Kiriesi, P.M. Ajayan, R. Vajtai, *Three-dimensional carbon nanotube scaffolds as particulate filters and catalyst support membranes.* ACS Nano, 2010(4): p. 2003-2008.

[19]. B.S. Amirkhiz, M.D., B. Simard, D. Mitlin, *Hydrogen sorption cycling kinetic stability and microstructure of single-walled carbon nanotube (SWCNT) magnesium hydride (MgH2) nanocomposite.* Journal of Physic chemistry, 2009(114): p. 3265-3275.

[20]. M. Penza, R.R., M. Alvisi, E. Serra, *Metal-modified and vertically aligned carbon nanotube sensors array for landfill gas monitoring applications.* Nanotechnology, 2010(21): p. 105501.

[21]. W.R. Small, M.I.H.P., *Inkjet printing of transparent, electrically conducting single walled carbon nanotube composites.* Small, 2007(3): p. 1500-1503.

[22]. M. Qian, T.F., K. Wang, H. Ding, Y.W. Chen, Z. Sun, *A comparative study of field emission properties of carbon nanotubes films prepared by vacuum filtration and screen printing.* Applied Surface Science, 2010(256): p. 4642-4646.

[23]. W.Wang, P.N.K., *Nanostructured hydrib silicon/carbon nanotube heterostructure: reversible high-capacity lithium-ion anodes.* ACS Nano, 2010(4): p. 2233-2241.

[24]. A.P.Graham, G.S.D., R.V. Seidel, M. Liebau, E. Unger, W. Pamler, F. Kreupl, W. Hoenlein, *Carbon nanotubes for microelectronic.* Small, 2005(1): p. 382-390.

[25]. L. Lacerda, A.B., M. Prato, K. Kostarelos, *Carbon nanotube cell translocation and delivery of nucleic acids in vitro and in vivo.* Journal of Material Chemistry, 2008(18): p. 17-22.

[26]. R. Fentona, K.D.C., *Fenton Reaction Controversy concerning the chemistry.* Ecological Chemistry and Engineering, 2009. **16**(3).

[27]. N.O. Nilvebrant, M.B.J., *Hydroxyl radical formation during hydrogen peroxide vleaching*. 2005.

[28]. J.M.O. Ramirez, A.M.J., O.J. Sandoval, R.C. Pless, *Hydrogen Generstion by Treatment of Aluminium Metal with Aqueous Solutions: Procedures and Uses*.

[29]. Fermani, S., et al., *Protein crystallization on polymeric film surfaces.* Journal of Crystal Growth, 2001. **224**(3-4): p. 327-334.

[30]. Fuchs, S. and C. Coester, *Protein-based nanoparticles as a drug delivery system: chances, risks, perspectives.* Journal of Drug Delivery Science and Technology, 2010. **20**(5): p. 331-342.

[31]. J. C Love, L.A.E., J K. Kriebel, R G. Nuzzo, G M. Whitesides, *Self-Assembled Monolayers of Thiolates on Metals as a Form of Nanotechnology.* Chemical Review, 2005(105): p. 1103-1169.

[32]. D. Cappus, C.X., D. Ehrlich, B. Dillmann, C. A. Ventnce Jr., K. Al Shamery, H. Kuhlenbeck and H.-J. Freund, *Hydroxyl groups on oxide surfaces: NiO(100),NiO(lll) andCr203(111).* Chemical Physics, 1993(177): p. 533-546.

[33]. X. Zou, X.L., Q. Zhao, S.Liu, *Synthesis of LaVO4/TiO2 heterojunction nanotubes by sol–gel coupled with hydrothermal method for photocatalytic air purification.* Journal of Colloid and Interface Science, 2012(1): p. 13-18.

[34]. U. G. Nielsen, H.J.J., J. Skibsted, *Small 51V chemical shift anisotropy for LaVO4 from MQMAS and MAS NMR spectroscopy.* Solid State Nuclear Magnetic Resonance, 2003(23): p. 107-115.

[35]. A. Patel, P.S., T. E. Rufford, V.Rudolph, Z. Zhu, *Selective catalytic reduction of NO with CO using different metal-oxides incorporated in MCM-41*. Chemical Engineering Journal, 2014(255): p. 437-444.

[36]. A. Patel, P.S., J.Chen, T. E. Rufford, S.Wang, V.Rudolph, Z. Zhu *Structural sensitivity of mesoporous alumina for copper catalyst loading used for NO reduction in presence of CO*. Chemical Engineering Research and Design, 2015.

[37]. J.Chen, F.C., R. Qu, X. Gao, K. Cen *Bimetallic cerium–copper nanoparticles embedded in ordered mesoporous carbons as effective catalysts for the selective catalytic reduction of NO with NH3.* Journal of Colloid and Interface Science, 2015(456): p. 66-75.

[38]. X. Yao, Y.X., W.Zou, L. Zhang, S. Wu, X. Dong, F.Gao, Y. Deng, C. Tang, Z. Chen, L. Dong, Y.Chen *Correlation between the physicochemical properties and catalytic performances of CexSn1–xO2 mixed oxides for NOreduction by CO.* Applied Catalysis B: Environmental, 2014(144): p. 152-165.

[39]. X.Wang, W.W., J. Mi, X. Li, R. Wang, *The ordered mesoporous transition metal oxides for selective catalytic reduction of NOx at low temperature,*. Applied Catalysis B: Environmental, 2015(176-177): p. 454-463.

[40]. B. Bhaduri, N.V., *Preparation of asymmetrically distributed bimetal ceria (CeO2) and copper (Cu) nanoparticles in nitrogen-doped activated carbon micro/nanofibers for the removal of nitric oxide (NO) by reduction.* Journal of Colloid and Interface Science, 2014(436): p. 218-226.

[41]. L. Dong, Y.T., B. Li, L. Zhou, F. Gong, H. He, B. Sun, C. Tang, F. Gao, L. Dong *Influence of molar ratio and calcination temperature on the properties of TixSn1 − xO2 supporting copper oxide for COoxidation.* Applied Catalysis B: Environmental, 2016(180): p. 451-462.

[42]. D. Gamarra, A.L.C., M. Monte, S.B. Rasmussen, L.E. Chinchilla, A.B. Hungría, G. Munuera, N. Gyorffy, Z. Schay, V. Cortés Corberán, J.C. Conesa, A. Martínez-Arias *Preferential oxidation of CO in excess H2 over CuO/CeO2 catalysts: Characterization and performance as a function of the exposed face present in the CeO2 support.* Applied Catalysis B: Environmental, 2013(130-131): p. 224-238.

[43]. T. Baidya, N.V.V., R. Verel, Y. Jiang, M. Yulikov, T. Kohn, G. Jeschke, A. Baiker, *SrO•Al2O3 mixed oxides: A promising class of catalysts for oxidative coupling of methane.* Journal of Catalysis, 2011(281): p. 241-253.

[44]. O.P. Tkachenko, A.A.G., A.V. Kucherov, K.C. Weston, A.M. Tsybulevski, L.M. Kustov, *Low-temperature CO oxidation by transition metal polycation exchanged low-silica faujasites.* Applied Catalysis B: Environmental, 2015(179): p. 521-529.

[45]. D.B.C. Venkata, S.S., H.r B. Friedrich, *Vanadium oxide supported on non-stoichiometric strontium hydroxyapatite catalysts for the oxidative dehydrogenation of n-octane.* Journal of Molecular Catalysis A: Chemical 2014(395): p. 398-408.

[46]. H. Lee, J.K.L., U. G. Hong, Y. Yoo, Y.J. Cho, J. Lee, H.S. Jang, J. C. J., I. K. Song *Effect of oxygen capacity and oxygen mobility of supported Mg3(VO4)2 catalysts on the performance in the oxidative dehydrogenation of n-butane.* Journal of Industrial and Engineering Chemistry, 2012(18): p. 808-813.

[47]. F. Li, F.X., B. Chen, Z. Huang, Y. Yuan, G. Yuan, *Direct catalytic conversion of glycerol to liquid-fuel classes over Ir–Re supported on W-doped mesostructured silica.* Applied Catalysis A: General, 2012(449): p. 163-171.

[48]. M.T. Pinho, H.T.G., R. S. Ribeiro, J. L. Faria, A. M.T. Silva, *Carbon nanotubes as catalysts for catalytic wet peroxide oxidation of highly concentrated phenol solutions: towards process intensification.* Applied Catalysis B: Environmental, 2015(165): p. 706-714.

[49]. Olajire, A.A., *Valorization of greenhouse carbon dioxide emissions into value-added products by catalytic processes.* Journal of CO2 Utilization, 2013(3-4): p. 74-92.

[50]. G. Zhou, H.L., H. Wang, H.Xie, G. Zhang, X. Zheng, *Catalytic combustion of PVOCs on MnOx catalysts.* Journal of Molecular Catalysis A: Chemical, 2014(393): p. 279-288.

[51]. J. Nie, X.W., Z. Ma, T. Xu, Z. Si, L. Chen, D. Weng, *Tailored temperature window of MnOx-CeO2 SCR catalyst by addition of acidic metal oxides.* Chinese Journal of Catalysis, 2014(35): p. 1281-1288.

[52]. M.S. Vasilyeva, V.S.R., A.Yu. Ustinov, M.A. Tsvetnov, *Formation, composition, structure, and catalytic activity in CO oxidation of SiO2 + TiO2/Ti composite before and after modification by MnOx or CoOx.* Surface and Coatings Technology, 2015(275): p. 84-89.

[53]. A. Zhang, Z.Z., J. Chen, W. Sheng, L. Sun, J. Xiang, *Effect of calcination temperature on the activity and structure of MnOx/TiO2 adsorbent for Hg0 removal.* Fuel Processing Technology, 2015(135): p. 25-33.

[54]. H. Zhao, G.Z., S. Chong, N. Zhang, Y.i Liu, *MnO2/CeO2 for catalytic ultrasonic decolorization of methyl orange: Process parameters and mechanisms,* . Ultrasonics Sonochemistry, 2015(27): p. 474-479.

[55]. X. Yang, C.D., R. Liu, J. Xie, D. Wang, *Balancing photovoltage generation and charge-transfer enhancement for catalyst-decorated photoelectrochemical water splitting: A case study of the hematite/MnOx combination.* Journal of Catalysis, 2013(304): p. 86-91.

[56]. D. Fang, J.X., H. Hu, H. Yang, F. He, Z. Fu *Identification of MnOx species and Mn valence states in MnOx/TiO2 catalysts for low temperature SCR.* Chemical Engineering Journal, 2015(271): p. 23-30.
[57]. H. Zhao, G.Z., Q. Zhang, *MnO2/CeO2 for catalytic ultrasonic degradation of methyl orange.* Ultrasonics Sonochemistry, 2014(21): p. 991-996.
[58]. M. T. Le, T.T.N., P. T. M. Pham, E. Bruneel, I. V. Driessche, *Activated MnO2-Co3O4-CeO2 catalysts for the treatment of CO at room temperature,.* Applied Catalysis A: General, 2014(480): p. 34-41.
[59]. S. Andreoli, F.A.D., C. Galletti, R. Pirone, *Nanostructured MnOx catalysts for low-temperature NOx SCR.* Chemical Engineering Journal, 2015(278): p. 174-182.
[60]. A Noorbakhsh, A.S., *Amperometric detection of hydrogen peroxide at nano-nickel oxide/thionine and Celestine blue nanocomposite-modified glassy carbon electrodes.* . Electrochimica Acta 2009(54): p. 6312-6321.
[61]. L.Wang, X.L., Y. Ye, La. Su, Y. Song. , *Nickel-cobalt nanostructure coated reduced grapheme oxide nanocomposite electrode for nonenzymatic glucose biosensing.* Electrochimica Acta 2013(114): p. 484-493.
[62]. D.Zhao, C.X.X., *A nanoporous palladium-nickel alloy with high sensing performance toward hydrogen peroxide and glucose.* Journal of colloid and Interface Science 2015(447): p. 50-57.
[63]. W. Sun, S.G., Y. Deng, T. Li, Y. Cheng, W. Wang, L. Wong, *Electrodeposited nickel oxide and grapheme modified carbon ionic liquid electrode for electrochemical myglobin.* Thin Solid Films, 2014(562): p. 653-658.
[64]. S. Lata, B.B., N.Karwasra, C. S. Pundir. , *An amperometric H2O2 biosensor based on cytochrome c immobilized onto nickel oxide nanoparticles/carboxylated multiwalled carbon nanotubes/polyaniline modified gold electrode.* Process Biochemistry 2012(47): p. 992-998.
[65]. P. Zhang, D.G., Q. Li, *Manganese oxide uultrathin nanosheets sensors for non-enzymatic detection of H2O2.* Material Letters 2014(125): p. 202-205.
[66]. H. Kivrak, O.A., D. Atbas, *Efficient and rapid microwave-assisted route to synthesize Pt MnOx hydrogen peroxide sensor.* . Electrochimica Acta, 2015(176): p. 497-503.
[67]. Y.W Hsu. T.K. Hsu, C.L.S., Y.T. Nien, N.W. Pu, M.D. Ger, *Synthesis of CuO/grapheme nanocomposites for nonenzymatic electrochemical glucose biosensor applications.* Electrochimicia Acta 2012(82): p. 152-157.
[68]. L.Q Luo, F.L., L.M Zhu, Z. Zhang, Y.P. Ding, D.M. Deng, *Non-enzymatic hydrogen peroxide sensor based on MnO2-ordered mesoporous carbon composite modified electrode.* Electrochimica Acta 2012(77): p. 179-183.
[69]. Y. han, J.B.Z., S.Y. Dong, *A novel nonenzymatic hydrogen peroxide sensor based on Ag-MnO2-MWCNT nanocomposites.* Electrochimica Acta 2013(90): p. 35-43.
[70]. D.L Zhou, J.J.F., L.Y. Cai, Q.X. Fang, J. R. Chen, A.J. Wang, *Facile synthesis of monodisperse porous Cu2O nanospheres on reduced grapheme oxide for non-enzymatic amperometric glucose sensing.* Electrochimica Acta 2014(115): p. 103-108.

[71]. Z.Y. Yu, H.J.L., X.M. Zhang, N.K. Liu, X.V. Zhang, *NiO/grapheme nanocomposite for determination of H2O2 with a low detection limit.* Talanta, 2015(115): p. 103-108.

[72]. Y.J. Yang, S.S.H., *Electrodeposited MnO2/Au composite film with improved electrocatalytic activity for oxidation of glucose and hydrogen peroxide.* Electrochimica Acta 2010(55): p. 3471-3476.

[73]. H.P. Peng, R.P.L., L. Zhang, J.D. Qiu. , *Sonochemical synthedis of magnetic core-shell Fe3O4@ZrO2 nanoparticles and their application to the highly effective immobilization of myoglobin for direct electrochemistry.* Electrochimica Acta 2011(56): p. 4231-4236.

[74]. D.X. Ye, H.X.L., G.H. Liang, J. Luo, X.X. Zhang, S. Zhang, H. Chen, J.L. Kong, *A three-dimensional hybrid of MnO2/grapheme/carbon nanotubes based sensor for determination of hydrogen-peroxide in milk.* Electrochimicia Acta 2013(109): p. 195-200.

[75]. Y. Tian, Y.L., W.P. Wang, X. Zhang, W. Peng, *CuO nanoparticles on sulfir-doped grapheme for nonenzymatic glucose sensing.* Electrochimica Acta 2015(156): p. 244-251.

[76]. P.M. Nia, W.P.M., F. Lorestani, M.R. Mahmaodian. Y. Alias, *Electrodeposition of copper oxide/polypyrrole/reduced grapheme oxide as a nonenzymatic glucose biosensor.* Sensors and Actuators B 2015(209): p. 100-108.

[77]. R. Rawal, S.C., Devender, C.S. Pundir, *An amperometric biosensor based on laccase immobilized onto Fe3O4NPs/cMWCNT/PANI/Au electrode for determination of phenoilic content in tea leaves extract.* Enzyme and Microbial Technology 2012(51): p. 179-185.

[78]. S.H. Kim, A.U., S.W. Hwang, *Rose-like CuO nanostructures for highly sensitive glucose chemical sensor application.* Ceramics International 2015(14): p. 9468-9475.

[79]. X.J. Chen, Y. Wang, C.Yan, *A novel bienzyme glucose biosensor based on three-layers Au-Fe3O4@SiO2 magnetic nanocomposite.* Sensors and Actutors B, 2011(159): p. 220-228.

[80]. K. Thandavan, S.G.N.N., S. Sethuraman, J.B.B. Rayappan, U,M. Krishnan, *Hydrogen peroxide biosensor utilizing a hybrid nano-interface of iron oxide nanoparticles and carbon nanotubes to assess the quality pf milk.* Sensors and Actuators B 2015(215): p. 166-173.

[81]. C. Karuppiah, M.V., S.M. Chen,S.H. Tsai, B.S. Lou, M. A. Ali, Fahad M.A. Al-Hemaid, *A simple hydrothermal synthesis and fabrication of zinc oxide-copper oxide heterostructure for the sensitive determination of nonenzymatic glucose biosensor.* Sensors and Actuators B 2015(221): p. 1299-1306.

[82]. K. Jindal, m.T., V. Gupta, *CuO thin film based uric acid biosensor with enhanced response characteristics.* Biosensors and Bioelectronic 2012(38): p. 11-18.

[83]. M. Tyagi, M.T., V. Gupta, *NiO nanoparticles-based urea biosensor.* Biosensors and Bioelectronics, 2013(41): p. 110-115.

[84]. K.Y. Hwa, B.S., *Synthesis of zinc oxide nanoparticles on grapheme-carbon nanotube hybrid for glucose biosensor applications.* Biosensors and Bioelectronics, 2014(62): p. 127-133.

[85]. R.M. Rioux, H.S., M. Grass, S. Habas, K. Niesz, J.D. Hoefelmeyer, P. Yang, and G.A. Somorjai, *Monodisperse platinum nanoparticles of well-defined shape: synthesis, characterization, catalytic properties and future prospects.* Topics in Catalysis 2006(39): p. 3-4.
[86]. C.D. Dong, C.W.C., C.F. Chen, C.M. Hung, *Scientific Reports 4*, in *5790*.
[87]. Mazan, I.P.S.L.M., *Formation of PVP-Protected Metal Nanoparticles in DMF*. Langmuir, 2002(18): p. 2888-2894.
[88]. Kochi, R.E.S.J.K., *Advances in Catalysis*. 2011, Academic Press INC (London) LTD.
[89]. Gibson, R.W.N.a.Q.H., *The reaction of ferrous horseradish peroxidase with hydrogen peroxide.* The journal of biological chemistry, 1970(10): p. 2409-2413.
[90]. D. Keilin, P.N., *Reactions of catalase with hydrogen peroxide and hydrogen donors.* Biochimica et Biophysica Acta, 1958(2): p. 302-307.
[91]. Powell, H.M. and S.T. Boyce, *Engineered Human Skin Fabricated Using Electrospun Collagen-PCL Blends: Morphogenesis and Mechanical Properties.* Tissue Engineering Part A, 2009. **15**(8): p. 2177-2187.
[92]. H. Theorell, A.E., *The reaction between catalase, azide and hydrogen peroxide.* Archives of Biochemistry and Biophysics, 1952(2): p. 462-474.
[93]. H.Theorell, A.E., B. Chance, *Electronic structure of the peroxidase-peroxide complexes.* Archives of Biochemistry and Biophysics, 1952(1): p. 237-239.
[94]. P. Holister, T.E.H., C. R. Vas, *Report on nanotube white papers*. 2003.
[95]. Varshney, K., *Carbon nanotubes: A review on synthesis, properties and applications.* International Journal of Engineering and General Science, 2014(2): p. 660-677.
[96]. Ijima, S., *Carbon nanotube.* Nature, 1991(56): p. 354.
[97]. Choi, Y., et al., *Development Of Novel Silk Fibroin-gelatin Bioink For 3d Cell Printing Technology.* Tissue Engineering Part A, 2014. **20**: p. S116-S116.
[98]. S.Zhu, G.X., *Single walled carbon nanohorns and their applications.* Nanoscale, 2010(2): p. 2538-2549.
[99]. Brenner, *Empirical potential for hydrocarbons for use in simulating the chemical vapor deposition of diamond films.* Physical Review, 1990. **15**(42): p. 365-366.
[100]. Calvert, P., *Strength in disunity.* Nature, 1992(357): p. 365-366.
[101]. T.W. Ebbesen, P.M.A., *Large scale synthesis of carbon nanotubes.* Nature, 2010(358): p. 220-222.
[102]. de Moraes, M.A., et al., *Silk fibroin and sodium alginate blend: Miscibility and physical characteristics.* Materials Science & Engineering C-Materials for Biological Applications, 2014. **40**: p. 85-91.
[103]. Y. Gagotsi, J.A.L., M. Yoshimura, *Hydrothermal synthesis of multiwall carbon nanotubes.* Journal of material Respiration, 2000(15): p. 2591-2594.
[104]. Y. Gogotsi, N.N., L. Libera, *In situ chemical experiments in carbon nanotubes.* Chemical Physic Letter, 2002(365): p. 354-360.
[105]. S. Manafi, H.N., H.R. Irani, *Low temperature synthesis of multiwalled carbon nanotubes via a sonochemical/hydrothermal method.* Materials Letter, 2008(62): p. 4175-4176.

[106]. C. Moreno, J.M.S., S.S. Fujino, T. Yoshimura, *Carbon nanocells and nanotubes grown in hydrothermal fluids.* Chemical Physical Letter, 2000(329): p. 317-322.
[107]. Harris, P., *Carbon nanotubes and related structures: new materials for the 21st century*, in *Cambridge University Press*. 1999.
[108]. H. Dai, A.J., E. Pop, D. Mann, Y. Lu, *Electrical transport properties and field-effect transistors of carbon nanotubes, NANO*. 2006. p. 1-4.
[109]. Sangwal, I.P.a.K., *Handbook of crystal Growth,Bulk Crsytal Growth: Basic techniques and Growth Mechanisms and Dynamics*. 2 ed.
[110]. Ahammad, A.J.S., *Hydrogen Peroxide Biosensors Based on Horseradish Peroxidase and Hemoglobin.* Journal of Biosensors and Bioelectronics, 2013(9): p. 1.
[111]. Kingzett, C.T., *Iodometric Titration.* Chemical News, 1880(41): p. 76.
[112]. C. Matsubara, N.K., K. Takamura, *Electrocatalytic Oxidation of Hydrogen Peroxide Based on the Shuttlelike Nano-CuO-Modified Electrode.* Analyst, 1992(117): p. 1781-1784.
[113]. Q.Chang, L.Z., G.Jiang, H. Tang, *Sensitive fluorescent probes for determination of hydrogen peroxide and glucose based on enzyme-immobilized magnetite/silica nanoparticles.* Analytical and Bioanalytical Chemistry, 2009(395): p. 2377-2385.
[114]. Y.Zhang, G.S.W., *Electrochemical oxidation of H2O2 on Pt and Pt + Ir electrodes in physiological buffer and its applicability to H2O2-based biosensors.* Journal Electroanal Chemistry, 1993(345): p. 253-271.
[115]. S.B Hall, E.A., Khudaish, A.L. Hart, *Electrochemical oxidation of hydrogen peroxide at platinum electrodes. Part 1. An adsorption-controlled mechanism.* Electrochimica Acta, 1998(43): p. 579-588.
[116]. Q.Wang, Y., Yun, J. Zheng, *Nonenzymatic hydrogen peroxide sensor based on a polyaniline-single walled carbon nanotubes composite in a room temperature ionic liquid.* Microchimica Acta, 2009(167): p. 153-157.
[117]. J.M. Zen, H.H.C., A.S. Kumar, *Facile synthesis of flower like copper oxide and their application to hydrogen peroxide and nitrite sensing.* Analyst, 2000(125): p. 1633-1637.
[118]. A.S. Kumar, S.S., *Electrocatalytic Reduction of Hydrogen Peroxide on Palladium-Gold Codeposits on Glassy Carbon: Applications to the Design of Interference-Free Glucose Biosensor.* Indian Journal of Chemistry, 2009. **48A**: p. 940-945.
[119]. M.Yemini, P.X., D.L. Kaplan, J. Rishpon, *Collagen-Like Peptide as a Matrix for Enzyme Immobilization in Electrochemical Biosensors.* Electroanalysis, 2006(18): p. 2049-2054.
[120]. J.Li, L.T.V., X.M. Liu, G.M. Zeng, G.H, Huang, G.L. Shen, R.Q. Yu, *Amperometric biosensor with HRP immobilized on a sandwiched nano-Au / polymerized m-phenylenediamine film and ferrocene mediator.* Analytical and Bioanalytical Chemistry, 2003(376): p. 902-907.
[121]. Unger, R.E., et al., *Vascularization and gene regulation of human endothelial cells growing on porous polyethersulfone (PES) hollow fiber membranes.* Biomaterials, 2005. **26**(17): p. 3461-3469.

[122]. J. Wang, X.C.Z., *Electrochemical sensors for environmental monitoring: a review of recent technology*. 2004, National Exposure Reaserch Laboratory, Office of research and development, U.S. Enviromental Protection Agency,.
[123]. Dyer, S.A., , *Survey of Instrumentation and measurement*. 2001: Wiley-Interscience John Wiley & Sons, Inc.
[124]. L.X. Yang, Y.J.Z., H. Tong, Z.H. Liang, L. Li, L. Zhang, *Hydrothermal synthesis of nickel hydroxide nanostructures in mixed solvents of water and alcohol.* Journal of Solid State Chemistry, 2007(80): p. 2095-2101.
[125]. C.H.Wu, J.S.M., C.H. Lu, *Synthesis and characterization of nickel-manganese oxide via the hydrothermal route for electrochemical capacitors.* Current Applied Physics, 2012(12): p. 1190-1194.
[126]. J. H. Lehman , M.T., E.Mansfield , K. E. Hurst, V.Meunier, *Evaluating the characteristics of multiwall carbon nanotubes.* CARBON, 2011(49): p. 2581 – 2602.
[127]. F. Doustan, A.A.H., M. A. Pasha, *Synthesis and Characterization of Carbon Nanotubes Catalyzed by TiO2 Supported Ni, Co and Ni-Co Nanoparticles via CCVD.* Journal of Nanostructures 2013(3): p. 333-339.
[128]. Ferrari, A.C., *Raman spectroscopy of graphene and graphite: Disorder, electron–phonon coupling, doping and nonadiabatic effects.* Solid State Communications, 2007(143): p. 47–57.
[129]. Thi Thanh Le Dang, M.T., *Polycrystalline NiO nanowires: scalable growth and ethanol sensing.* Procedia Engineering 2015(120): p. 427-434.
[130]. N. Adeela, K.M., U. Khan, S. Karim, M. Ahmad, M. Iqbal, S. Riaz, X.F. Han, M. Maqbool, *Fabrication and temperature dependent magnetic properties of nickel nanowires embedded in alumina templates.* Ceramics International 2015(41): p. 12081-12086.
[131]. Azhar Z. Abbasi, P.P., PingCai, ChunshengHe, Warren D. Foltz, Mohammad Ali Amini, Claudia R. Gordijo, AndrewM.Rauth, Xiao Yu Wu, *Manganese oxide and docetaxel co-loadedfluorescent polymer nanoparticles for dual modal imaging and chemotherapy of breast cancer.* Journal of Controlled Release 2015(209): p. 186-196.
[132]. Masoud Salavati-Niasaria, F.D., Mehdi Mazaheri, *Synthesis of Mn3O4nanoparticles by thermal decomposition of a [bis(salicylidiminato)manganese(II)] complex.* Polyhedron, 2008(27): p. 3467-3471.
[133]. Kheiri, N.T.a.M., *Sol-gel derived nanostructured nickel oxidefilms: Effect of solvent on crystallographic orientations.* Solid States Sciences 2014(27): p. 79-83.
[134]. S.J. Ahmadpanah, M.S., J. S. Ahari, M. Kakavand, *Study of Parameters Affecting the Crystal Size Distribution of Sodium Chloride in Bench scale Crystallizers.* Petroleum & Coal 2007(1): p. 54-60.
[135]. Abbona, F., *Crystal growth of Technology Important Electronic Materials*. p. 89-117.
[136]. D. Mohammadyani, S.A.H., S.K. Sadrnezhaad, *Characterization of Nickel Oxide Nanoparticles Synthesized Via Rapid Microwave-Assisted Route.* International Journal of Modern Physics, 2012(5): p. 270-276.
[137]. M.Yersoh, A.S., *Handbook of Industrial Crystallization*. 2 ed.

[138]. Govindhan Dhanaraj, K.B., Vishwanath Prasad *Springer Handbook of Crystal Growth*. 2010: Science. 1. S. Su, W.W., J. Gao, J. Lub, C. Fan, *Nanomaterials-based sensors for applications in enviromental monitoring.* Journal of Materials Chemistry, 2012. **22**(35): p. 18101-18110.

[139]. G. Bai, H. Dai, J.Deng, Y. Liu, W. Qiu, Z. Zhao, X.Li, H. Yang T*he microemulsion preparation and high catalytic performance of mesoporous NiO nanorods and nanocubes for toluene combustion* . Chemical Engineering Journal, 2013 (219): p. 200-208

[140]. W.Zeng, B. Miao, L.Y. Lin, J.Y. Xie, *Facile synthesis of NiO nanowires and their gas sensing performance*. 2012 (22): p. 100-104

[141]. B. Lu, J. Bai, X. Bo, L. Zhu, L. Guo, *A simple hydrothermal synthesis of nickel hydroxide–ordered mesoporous carbons nanocomposites and its electrocatalytic application* . Electrochimica Acta, 2010 (28): p. 8724-8730

[142]. L. Zhou, J. Zhang, J.He, Y. Hu, H. Tian, *Control over the morphology and structure of manganese oxide by tuning reaction conditions and catalytic performance for formaldehyde oxidation.* Materials Research Bulletin, 2011 (10): p. 1714-1722

APPENDIX

VITA

Suriani Binti Ibrahim is a PhD student at Chulalongkorn University under Electrical Engineering Department. She got scholarship under AUNSeed-Net sandwich programme. Her thesis title is Binary Catalyst for Amperomteirc Biosensors.